

MAGNETIC COUPLINGS IN ORGANIC-INORGANIC HYBRIDS

Hybrid Materials are composed of both inorganic and organic moieties. They are promising materials because characteristics of both organics and inorganics can be combined to design materials with multiferroics character. The magnetic and electronic properties are interesting for applications like energy transfer or data storage. Especially the hybrids with a layered organic-inorganic structure are interesting. The inorganic layers are confined in one direction to form layers of two-dimensional magnets. An ab-initio study is performed to investigate the magnetic properties and magnetic structure of layered hybrids. The magnetic interactions are very weak and subtle hence the magnetic properties are investigated by advanced computational methods. An embedded cluster approach is used and multi-configurational methods like CASSCF, CASPT2 and DDCI are applied to calculate the magnetic couplings. The outcome of these embedded calculations elucidated the magnetic structure.

Supervisors: Prof. dr. H.B. Broer & dr. R.W.A. Havenith
Referee: Dr. G.R. Blake

CONTENTS

Introduction.....	2
Research Question	3
The CRYSTAL Structure.....	3
An Organic-Inorganic Hybrid (OIH)	3
The crystals	4
Theoretical considerations and Methods	7
Periodic Calculations.....	7
Embedded cluster method	9
Cluster Calculation Methods.....	10
Basis sets & Relativity.....	14
Other.....	14
Magnetic coupling determination	14
Magnetic exchange.....	17
Results & Discussion	20
One Atom.....	20
MnCl ₄ Methyl Amine.....	23
MnCl ₄ Phenyl Ethyl Amine.....	35
FeCl ₄ Methyl Amine	37
Other considerations	39
Conclusion	40
Acknowledgements	40
References	41
Appendices.....	43
Appendix A – Crystal structures	43
Appendix B – AIMPS.....	44
Appendix C - Manual	49
Appendix D– Data Sets	51

INTRODUCTION

Organic Inorganic Hybrids (OIHs) are promising materials: properties of the inorganic and organic world are combined in order to produce materials with multiferroic properties. Multiferroics are materials that have both ferromagnetic and ferroelectric character. This indicates that the materials have a finite magnetic and an electric polarization at low temperatures. The magnetic-electric behavior of the OIHs depends strongly on both the inorganic and organic part.¹

It is expected that OIHs can be used for data transport and data storage. They are also interesting because their production is rather straightforward. Moreover the materials are cheap which makes them eventually useful for single-use electronics.^{2,3}

Perovskite based OIHs are ideal for multiferroic materials. In most cases the OIHs have a three dimensional structure. Here we will instead focus on layered structures. In this case a quantum confined low dimensional structure is created consisting of layers of 2 dimensional magnets separated by an organic layer. We will investigate the magnetic behavior of these materials.¹

We focused on materials containing either iron or manganese. They consist of alternating sheets of perovskites and sheets of organic molecules with an amine group bonded via Coulombic and dispersive interactions.

Magnetism is understood as aligned spins. This alignment depends on the interaction of magnetic centers with each other. This interaction is called the magnetic coupling. These magnetic couplings are mostly very small hence high-precision methods need to be used. In most cases periodic calculations are not sophisticated enough to treat the complexity needed to calculate the magnetic couplings accurately.

The alternative of periodic calculations is to use an embedded cluster approach. A small part of the crystal is extracted and the surrounding crystal is mimicked using potentials. After that only the inner part is treated quantum mechanically.

Open shell metal systems cannot be treated well using Hartree-Fock (HF) and Density Functional Theory (DFT). Therefore multi-configurational post-HF methods are used like Complete Active Space -Self Consistent Field (CAS-SCF), Second order Perturbation Theory (CAS-PT2) and Difference Dedicated Configuration Interaction (DDCI).

The outline of this thesis is as follows: First the materials are described. Secondly the methodology is explained. Afterwards the results are given and discussed followed by a conclusion.

RESEARCH QUESTION

The aim of this project is to understand the magnetic structure of two-dimensional layered OIHs. A good understanding of the magnetic structure will give us insight in the mechanism of 2-dimensional magnetism and will provide insight of the design of new multiferroics materials. We would like to determine and understand the magnetic couplings within and between the inorganic sheets, qualitatively but also quantitatively.

THE CRYSTAL STRUCTURE

AN ORGANIC-INORGANIC HYBRID (OIH)

There exists a tremendous variety of organic-inorganic hybrid materials. Some of them are only hybrid in the sense that they are 'mixed' on larger scale. Regarding only OIHs that are hybrids on molecular scale one can make a distinction between them based on the dimensionality of the connectivity within the organic and within the inorganic parts.³

In this thesis we studied OIHs that have a layered topography. In this case a structure is created that shows specific 2 dimensional properties.¹ The OIHs consist of alternating organic and inorganic layers. The inorganic layers are formed by (001) planes of perovskites. Perovskites are crystal structures with corner shared octahedrons of halogen ligands filled with a metal atom. The metals have a 2+ charge, M^{2+} , and the ligands are negatively charged, X-. In our cases the ligands are chlorine atoms, two thirds of them acting as bridging ligands between the metal cations and one third of the chlorines pointing towards the organic part.⁴

The organic layer consists of two layers of organic molecules with a positively charged amine group pointing towards the negatively charged inorganic layer. (see fig. 1).

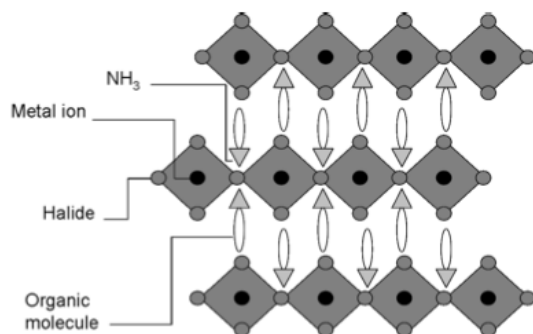


Fig. 1 Schematic representation of the hybrid structure with exaggerated interdigitation of the organic part.²⁵

With this basic two dimensional OIH structure a lot of variations can be made. Both the inorganic and organic part can be changed. For the metal ion one can use for example Cu^{II} , Fe^{II} , Mn^{II} , Pb^{II} . For the inorganic ligand one can use Cl^- , Br^- , or I^- and for the organic parts all kinds of different amine containing molecules can be used. All these different materials show different optical, magnetic and electric properties. For example the iron and manganese based hybrids show antiferromagnetic behavior while the lead and copper based hybrids show often ferromagnetic behavior.⁵ Also the dielectric properties can change significantly by changing the chain lengths of the organic layer.⁶ The relationship between the properties and the materials is a very complex one. This is illustrated by the fact that the organic ligands influence the magnetic coupling of the inorganic part.

One of the advantages of hybrid materials is that they can be produced very easily: the organic ammonium salt (R-NH₃Cl) and the inorganic salt (MCl₂) are dissolved in a 1:2 ratio in ethanol or acetone and the solution is crystallized in a refrigerator. It is also possible to spin-coat the material and therefore they can be used as printable electronics.^{4,7}

The crystal structures of the hybrid materials are often determined via powder X-ray diffraction. Also Raman and IR spectroscopy are used to determine the atomic positions. Via X-ray spectroscopy an electron density is obtained of the crystal. The atomic positions are determined from the obtained electron density. Due to the fact that the electron density on a hydrogen atom (only one electron) is small relative to the other atoms, the positions of the hydrogen atoms are often invalidly determined. For this reason the hydrogen positions are optimized computationally.⁶

THE CRYSTALS

The three crystals that are used are given below together with the abbreviations that are used.

1. MnCl₄(CH₃NH₃)₂ - MNMA
2. MnCl₄(C₆H₅C₂H₄NH₃)₂ - MNPEA
3. FeCl₄(CH₃NH₃)₂ - FEMA

Most attention is paid to MNMA. The effect of changing the organic layer is investigated by looking at MNPEA. Moreover the effect of changing the manganese atoms to iron atoms is investigated by looking at FEMA.

MNMA

The unit cell of MNMA is tetragonal meaning that $\alpha=\beta=\gamma=90^\circ$ and $a=b$. The cell parameters are $a=b=7,1999(2)$ Å and $c=19,2744(7)$ Å and the cell volume $999,15$ Å³. The crystallographic point group is specified as 138: $P4_2/ncm$. The P indicates a primitive Bravais lattice. The 4_2 indicates that there are screw axes along the axes of the unit cell. The screw axes consist of a rotation of $\frac{360}{4}$ degrees and a translation of a $\frac{2}{4}$ axis. The **n** indicates a glide plane on half of the diagonal of a face, the **c** a glide plane along half the lattice vector of this face, and **m** indicates a reflection plane. In fig. 3 all symmetry elements are indicated.

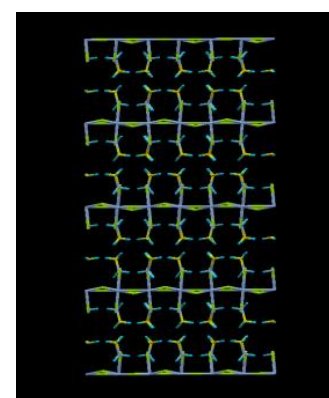
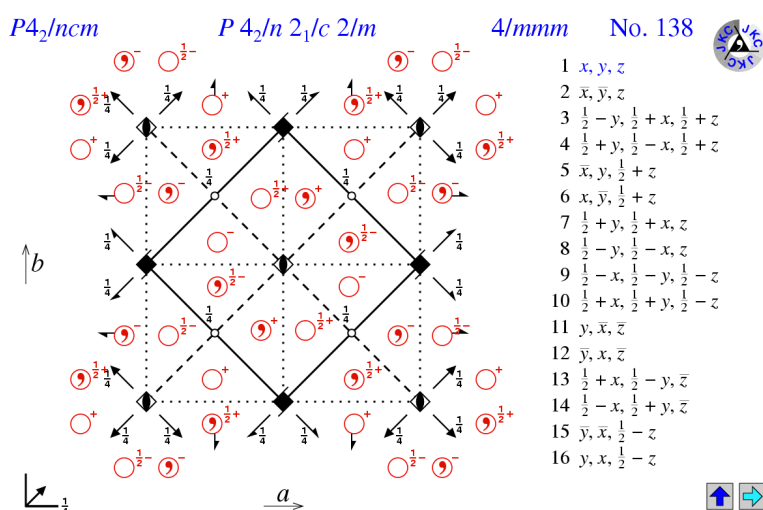


Fig. 2 Part of the MNMA crystal viewed from the [110] direction. The layered structure is well visible here.

Fig. 3 Schematic representation of the symmetry elements in point group 138⁸

The MNMA crystal consists of perovskite sheets of Mn²⁺ and Cl⁻ ions. The chlorine anions have a closed shell configuration [Ar] and the manganese cations have an empty 4s shell [Ar]3d⁵. The manganese cations have five open shell electrons in the 3d shell; this gives rise to unusual high spin configurations with a sextet multiplicity.

The MNMA has a buckling angle in alternately the $[110]$ and $[\bar{1}10]$ direction. This means that the perovskite sheets are not parallel to the c axis of the crystal but are canted (see fig 4). This can give rise to canted anti-ferromagnetism. This is also observed experimentally for layered manganese crystals having a ferromagnetic moment parallel to the planes below 40-45 K.⁹

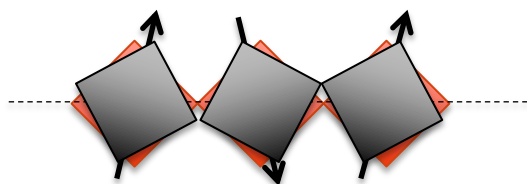


Fig. 4 Schematic representation of the buckling angle and the anti-ferromagnetically aligned spin vectors

The origin of the buckling angle is the interaction of the negative chlorine atoms with the positively charged amine groups of the methylamine. There is an $N^+-H\cdots Cl^-$ interaction; strictly speaking this cannot be called a hydrogen bond because the Cl^- is too large and the interaction is mainly electrostatic between the nitrogen and chlorine atom.¹⁰ The chlorine atoms move towards the amine group as depicted in fig 5. The amine groups influence the interactions with the chlorine atoms and so induce a buckling angle that influences the magnetic interactions in the perovskite sheets.¹

Although the buckling angle has a small effect on the magnetic coupling itself, a larger angle gives a larger canting of the spin magnetic moment. A small increase in buckling angle can therefore give a significant increase in the net magnetic moment.

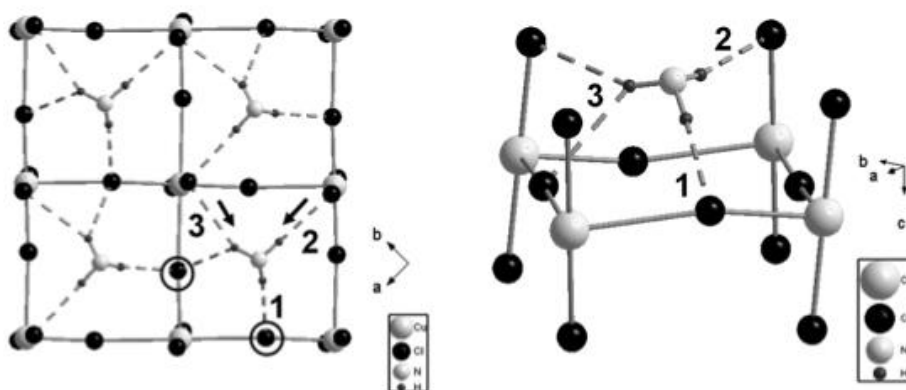


Fig. 5 The $N^+-H\cdots Cl^-$ attractions viewed from the top (left) and from the side (right)⁵

Adjacent inorganic layers are symmetrically related to each other by a rotation of 90° and a translation of $(\frac{1}{2}, \frac{1}{2}, \frac{1}{2})$. This makes it difficult to guess the magnetic interaction between magnetic centers between inorganic sheets because for each Mn in one sheet there are four nearest Mn atoms in both the adjacent sheets. (fig. 6)

The in-plane Mn-Mn distance is 5,09 Å, while the intra plane Mn-Mn distance is double of it, 10,29 Å. The vertical inter plane distance is 9,6 Å. Due to the buckling angle the Mn-Cl distances in the 110 , $1\bar{1}0$ and the 001 direction are not the same. They are 2,546 Å, 2,571 Å and 2,493 Å respectively. The distance between the nitrogen atom and the magnetic manganese centers is 4.129 Å.

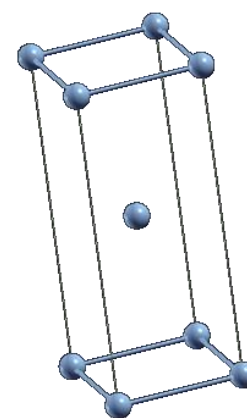


Fig. 6 Schematic representation of how the metal centers are related to each other emphasizing that there are eight nearest neighbors in the adjacent inorganic sheets

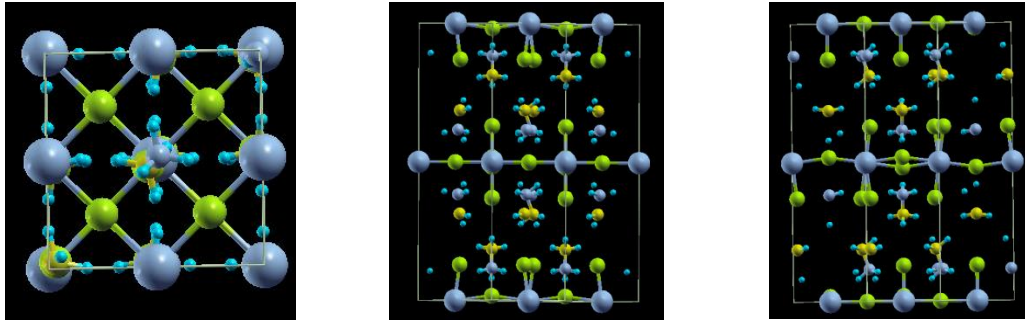


Fig. 7 MNMA viewed from the top [001], from the *a* side [100] and from the *b* side [010] respectively

MNPEA

The unit cell of MNPEA is orthorhombic $\alpha=\beta=\gamma=90^\circ$. The lattice parameters are $a=7,1480(6) \text{ \AA}$, $b=7,1697(7) \text{ \AA}$ and $c=39.088(4) \text{ \AA}$ with a cell volume of $2003,2 \text{ \AA}^3$. The crystallographic point group is 19: $P2_12_12_1$. The P indicates a primitive Bravais lattice and 2_1 (\uparrow) indicates a two-fold screw axis: a rotation of 180° and a translation of a $\frac{1}{2}$. In fig. 8 all symmetry elements are shown; there are significantly less symmetry elements than for the point group of MNMA.

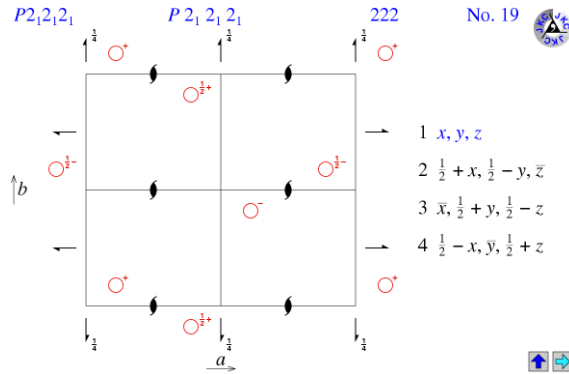


Fig. 8 Schematic representation of the symmetry elements in point group 19⁸

The inorganic structure of MNPEA has a lot of similarities with MNMA but it is slightly different in the fact that there is a buckling angle in both the $[110]$ and $[\bar{1}10]$ direction for each particular sheet. (fig. 10)

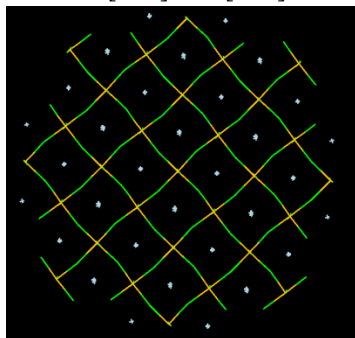


Fig. 10 An inorganic perovskite sheet emphasizing the buckling angle. The blue dots are the nitrogen cations from the PEA molecules.

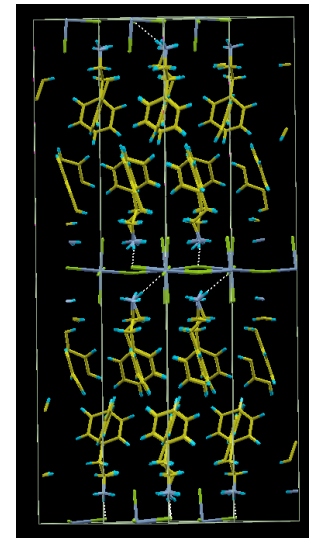


Fig. 9 A part of a MNPEA crystal showing that the phenyl groups are oriented perpendicular and parallel in different directions

Phenyl ethylamine is much larger than methylamine so the interlayer distance is much larger and so the magnetic coupling between the layers is expected to be very small.

The phenyl rings are oriented to each other in a so-called herringbone structure. In this structure the adjacent phenyl rings are perpendicular to each other. Phenyl groups in a herringbone structure can show interesting electronic behavior.

FEMA

FEMA has a tetragonal unit cell, as has MNMA. The lattice parameters are $a=b=7,1325(6)$ Å and $c=19,0193(17)$ Å. These are slightly smaller compared to the MNMA unit cell which ones are $7,1999$ Å and $19,2744$ Å respectively. The in-plane Fe-Fe distance is $5,04$ Å. This is only $0,01$ Å smaller than the Mn-Mn distance in MNMA. The cell volume is $967,56$ Å³. The crystallographic point group is specified as $P4_2/ncm$, the same as for MNMA.

FEMA has also a buckling angle in one direction as in MNMA. The buckling angle is 166° and so a bit less sharp than MNMA crystal. The iron atoms have a 2+ charge making their electronic configuration $[Ar]3d^6$. A single iron atom in a high spin state configuration has quintet multiplicity.

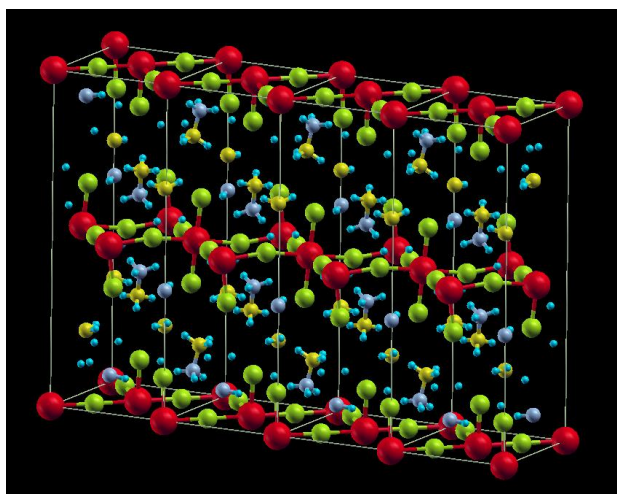


Fig. 11 A $[411]$ supercell of a FEMA crystal

THEORETICAL CONSIDERATIONS AND METHODS

PERIODIC CALCULATIONS

The periodic calculations were performed using the CRYSTAL09 package.^{11,12} CRYSTAL is able to perform ab-initio SCF and DFT calculation on ground states. CRYSTAL has a good scaling in running jobs parallel over more than 100 cores.

Periodic calculations were used for a few reasons. First the positions of the hydrogens needed to be optimized because they are only roughly guessed from XRD spectra. Secondly the magnetic couplings were calculated to obtain some insight in the magnetic structure and to get some values to validate the embedded cluster method.

The input geometries of the crystals were obtained from X-ray spectra determined at 100 K. The resulting .cif-files were read using PLATON.¹³ The position of the hydrogen atoms were optimized keeping the other atoms, the symmetry and the cell parameters fixed. For the coordinates of the crystals see Appendix A.

All CRYSTAL calculations were carried out within the framework of DFT using the Perdew-Burke-Ernzerhof (PBE) functional.¹⁴ In this functional the density gradient,¹⁵

$$x(r) = \frac{\nabla\rho(r)}{\rho^{4/3}(r)} \quad (1)$$

is taken into account, called the generalized gradient approximation. PBE is free of empirical parameters.

The basis sets for the periodic calculations were obtained from the CRYSTAL basis set library:

1. Fe_86-411d41G_towler_1992a
2. Mn_86-411d41G_towler_1992
3. Cl_86-311G_apra_1993
4. C_6-21G*_catti_1993
5. N_6-21G*_dovesi_1990
6. H_5-11G*_dovesi_1984

To achieve convergence some tricks have been used. A **level shift** was used to shift the virtual energy levels up for a half hartree. Also the spin was initially locked in the high spin state. Because of the fact that the energy differences of different spin states are small, high precision is required. The truncation of bielectronic integrals was lowered four orders of magnitude and the convergence threshold on the total energy was also lowered from 10^{-6} to 10^{-10} . For the low spin states the spin of specific atoms in the cell were flipped from alpha to beta spins breaking the symmetry of the crystal.

GRIMME DISPERSION CORRECTION

Within the framework of (periodic) DFT it is difficult to calculate VanderWaals forces. These attractive forces of induced dipoles calculated via DFT are too low. For this reason one can use a Grimme correction.¹⁶ This is a semi-empirical pair potential added to the DFT energy. It does not really describe the dispersion interaction but tries to model it in a computationally appropriate way. This correction includes a set of empirical parameters for each different functional and atomtype. The Grimme dispersion as implemented in the CRYSTAL09 package is written as:¹¹

$$E_0 = E_{KSDFT} + E_{Dispersion}$$

$$E_{dispersion} = -s_6 \sum_{i=1}^{Nat-1} \sum_{j=i+1}^{Nat} \sum_g \frac{C_6^{ij}}{R_{ij,g}} f_{dump}(R_{ij,g})$$

In which f_{dump} is:

$$f_{dump}(R_{ij}) = \frac{1}{1 + e^{-d(\frac{R_{ij}}{R_r}-1)}}$$

The summation is over each atom pair and lattice vectors, \mathbf{g} . C_6^{ij} is the dispersion coefficient, s_6 a scaling factor depending on the used functional and R is the interatomic distance. For each atom pair the C_6 coefficient is given as the geometrical mean of the C_6 coefficients of the atom types:

$$C_6^{ij} = \sqrt{C_6^i C_6^j}$$

The C_6 parameters used are derived from table 1 in ref. [16]

Atom	C_6 (Jnm ⁶ mol ⁻¹)
H	0.14
C	1.75
N	1.23
Cl	5.07
Mn	10.80

The Grimme correction is applied to the periodic calculations of the MNPEA structure and to a benzene crystal. Both structures have a herringbone orientation of aromatic rings.

EMBEDDED CLUSTER METHOD

There are a lot of chemical properties that cannot be determined only by a description of the ground state. Moreover in metals the electronic states are often multi-configurational in character. For this reason we need to apply methods that treat multiple configurations. We can do this via the embedded cluster approach.

In the embedded cluster approach only a small part of the crystal is extracted. An energy potential is constructed to mimic the rest of the crystal. A first approximation is to mimic the potential field of the crystal by a set of point charges, called the Madelung field. This Madelung potential is added to the Hamiltonian.¹⁷

$$\hat{H} = \hat{H}_{cluster} + \hat{V}_{Madelung} \quad (1)$$

The Madelung field is made with the Ewald method as implemented in the MadPot program.¹⁸ First the crystal field is calculated from the crystal structure on a grid and secondly the effect of the cluster itself is subtracted from that. Thirdly a set of point charges within a certain radius from the cluster is created and they are fitted to the exact Madelung field.

To increase the quality of the embedding, spherical model potentials are placed between the cluster and the Madelung field. These potentials are called Ab-Initio Model Potentials (AIMPs) and they describe not only the electrostatic interactions of the ionic sites (Madelung field) but also take into account the electrostatic potential of the electron density, the exchange interaction between the cluster and the embedding electrons and the quantum mechanical Pauli repulsion operator.^{19,20}

$$\hat{H} = \hat{H}_{cluster} + \hat{H}_{AIMP} + V_{Madelung} \quad (2)$$

With

$$\hat{H}_{AIMP} = \sum_i^{N_{e,clus}} \sum_e^{N_{ions,env}} \left[-\frac{Z_e - N_e}{r_{ei}} + V_{coul}^e(i) \right] + [V_{ex}^e(i) + P^e(i)] \quad (3)$$

The summation is over all electrons of the cluster, $N_{e,clus}$ and all nuclei, N_{ions}

AIMPs are different for each material hence they have to be created for each crystal that is used. They are made using the SCEI, Self-Consistent Embedding Ions procedure.¹⁹ Within this procedure a simple HF calculation is performed on the ground state of a single ion within a spherical part of the crystal surrounded by a Madelung field. An initial AIMP is produced that is used in the subsequent calculations until the total energies and orbital energies are converged. (More computational details about the process of making AIMPs are in appendix B and C.)

CLUSTER CONSTRUCTION:

The choice of the cluster needs some crucial considerations. On one hand the cluster must not be too small to describe the physics that takes place but on the other hand the cluster cannot be too large in order to be able to treat electron correlation in a proper way. When the cluster is too large the calculations will become too expensive.

As a guide for a cluster in which one wants to calculate magnetic interactions, one needs at least the magnetic metal centers, the bridging ligands and the first shell of nearest neighbors. AIMPs are then placed on all second nearest neighbor positions.

TESTING THE CLUSTER, UHF/DFT

When the AIMP's and the Madelung field are constructed the embedded approach needs to be verified. This is done by comparing calculations of the magnetic coupling periodically and with the embedded cluster approach. These calculations are performed using both DFT/PBE and the basis sets from the CRYSTAL basis set library as mentioned before.

CLUSTER CALCULATION METHODS

Below the methods that are used on the embedded cluster are explained. All embedded cluster calculations are performed using MOLCAS²¹ except the DDCI calculations. The DDCI calculations are performed with the DIESEL²² package however the reference wavefunction is also calculated with MOLCAS.

In the DDCI and CASPT2 calculations the core orbitals are frozen so they are always doubly occupied; hence no excitations from the frozen orbitals are considered.

The frozen orbitals are typically all the orbitals that do not belong to the valence shell. For carbon and nitrogen the 1s orbital is frozen. For chlorine, iron and manganese the 1s, 2s and 2p orbitals are frozen.

SDCI:

A wavefunction has to obey the Pauli exclusion principle and has to be antisymmetric. A simple way to do this is to use orthonormal Slater determinants.

$$\Psi_0^{el} = \begin{vmatrix} \psi_1(x_1) & \cdots & \psi_n(x_1) \\ \vdots & \ddots & \vdots \\ \psi_1(x_N) & \cdots & \psi_n(x_N) \end{vmatrix} = |\psi_1(x_1) \cdots \psi_n(x_N)| \quad (4)$$

Also single and double excited determinants can be constructed:

$$\Psi_i^p = |\psi_1 \cdots \psi_{i-1} \psi_p \psi_{i+1} \cdots \psi_n(x_N)| \quad (5)$$

$$\Psi_{ij}^{pq} = |\psi_1 \cdots \psi_{i-1} \psi_p \psi_{i+1} \cdots \psi_{j-1} \psi_q \psi_{j+1} \cdots \psi_n(x_N)| \quad (6)$$

In the same manner multiple excited determinants can be constructed. Finally we can express the exact Full-Configuration-Interaction (FCI) wavefunction as:

$$\Psi = C_0 \Psi_0 + \sum_{i,p} C_i^p \Psi_i^p + \sum_{\substack{i<j \\ p<q}} C_{ij}^{pq} \Psi_{ij}^{pq} + \sum_{\substack{i<j<k \\ p<q<r}} C_{ijk}^{pqr} \Psi_{ijk}^{ppr} + \cdots \quad (7)$$

The values of the coefficients can be obtained by solving the secular equations. However except for small molecules the FCI expansion is so large that one has to truncate. Often only the single and double excitations are taken into account (SDCI).

For a FCI the number of determinants can be calculated by

$$D_{determinants}(n, N, S) = \binom{n}{N/2 + S} \binom{n}{N/2 + S} \quad (8)$$

And the number of CSFs can be calculated by Weyl's dimension formula:

$$C_{CSF}(n, N, S) = \frac{2S + 1}{n + 1} \binom{n + 1}{N/2 - S} \binom{n + 1}{N/2 + S + 1} \quad (9)$$

Here n is the number of orbitals, N the number of electrons and S the total electron spin. To show how the number of CSFs and determinants grow the number of CSFs and determinants of the lowest spin state are calculated for a FCI space with $N=n$ from 1 to 10.

Table 1 The number of CSFs and determinants for n electrons in N orbitals, with $N=n$

(N,n)	Spin, S	C CSFs	D Det.'s
1	$\frac{1}{2}$	1	1
2	0	3	4
3	$\frac{1}{2}$	8	9
4	0	20	36
5	$\frac{1}{2}$	75	100
6	0	175	400
7	$\frac{1}{2}$	784	1225
8	0	1764	4900
9	$\frac{1}{2}$	8820	15876
10	0	19404	63504

CORRELATION ENERGY:

The energy difference between the HF energy and the FCI energy is called the correlation energy. The correlation energy can be divided in a dynamical and a static part. The dynamic correlation concerns the effects caused by the movement of the electrons, especially the Pauli repulsion between electrons of opposite spins. To take this interaction into account a lot of other determinants are mixed in to enable the electrons to adapt to each other. This correlation is mainly treated by perturbation theories, CI and CC methods.

The static correlation or non-dynamical correlation is the energy that is concerned with a ground state that cannot be properly described with a single configuration because there are more than one configurations with the same or almost the same energy. The static correlation can often be taken into account by performing a MCSCF calculation.

MCSCF:

The Hartree-Fock (HF) method only considers one ground state configuration. However many molecular properties are multi-configurational in character, especially in magnetic systems with open d shells. For this reason multi-configurational SCF (MCSCF) methods are used.

CASSCF:

One important multi-configurational method is the Complete Active Space (CAS) approach. In CASSCF the orbitals are divided in an inactive space with all doubly occupied orbitals, a virtual space with no occupation and the active space with no restrictions on the occupation. Within the active space an FCI is performed. Iteratively, the expansion coefficients are optimized simultaneously with the orbital coefficients from the SCF. CASSCF is primarily used for a proper description of the multi-configurational ground state hence concerns the static electron correlation. The size of the active space is often represented as $[n,m]$ with n the number of electrons and m the number of orbitals.

Choice of the active space:

The number of configurations of the CAS grows very fast by increasing the size of the active space, therefore the active space has to be as small as possible. However the CAS needs to include all configurations to describe the system properly. Especially for low spin states the number of configurations increases very rapidly. It is often a good option to include all the valence orbitals in the active space although for medium-sized systems this becomes already an unmanageable space. The lowest unoccupied and highest occupied orbitals of a simple HF calculation give often, but not necessarily, the most important orbitals.

In our calculations we take into account all the valence d orbitals of the metal atoms. This is usually a good choice but the number of configurations can increase very fast. In the table below the number of determinants and CSFs are shown for a CAS(10,10) for different multiplicities.

Table 2 The number of CSFs and determinants for 10 electrons in 10 orbitals

Spin, s	Mult	C CSFs	D det. 's
0	1	19404	63504
1	3	29700	44100
2	5	12375	14400
3	7	1925	2025
4	9	99	100
5	11	1	1

As you can see the number of CSFs and determinants increases rapidly by going from high to low multiplicity.

CASPT2

After the CASSCF procedure it is possible to calculate a larger part of the dynamical correlation via perturbation theory where the CASSCF wavefunction is used as the reference. The energy expression up to the second order perturbation theory is:

$$E_i = E_i^{(0)} + \langle \Psi_i | \hat{V} | \Psi_i \rangle^{(1)} + \sum_{j \neq i} \frac{\langle \Psi_i | \hat{V} | \Psi_j \rangle \langle \Psi_j | \hat{V} | \Psi_i \rangle^{(2)}}{E_i^{(0)} - E_j^{(0)}} \quad (10)$$

For CASPT2 the CASSCF wavefunction is used as the reference function instead of a single determinant wavefunction as in MP2. Perturbation theory is not variational and therefore the variational theorem does not apply here. For this reason the CASPT2 energies can also be lower than the exact energy (FCI).

One drawback of the CASPT2, which is general for perturbation theory, is the possibility of intruder states.²³ These are unphysical states that give a large contribution in the total energy expression because they have a small energy difference, and so a small denominator. To check that there are no intruder states one can check the contribution of terms with a small denominator and one can check whether the contribution of the reference wavefunction is large enough via:²³

$$\omega = (1 + \alpha)^{-\frac{N}{2}} \quad (11)$$

N is the number of correlated electrons and α is a measure of the contribution to the correlation energy per single electron pair. We assume that α is approximately 0.015. When the reference weight of the calculation is much less lower the expected reference weight ω there are intruder states. For a structure with more than 90 correlated electrons the reference weight is already only approximately 50% of the total wavefunction.

Another more extensive multi-configurational treatment is the Difference Dedicated Configuration Interaction (DDCI) method. This method does not primarily focus on getting highly accurate absolute energies but focusses on the relative energy between various states.^{24,25}

DDCI is a method developed to describe properties like the ionization potential, electron affinity, optical transitions and magnetic exchange coupling. Especially the latter is relevant for now.

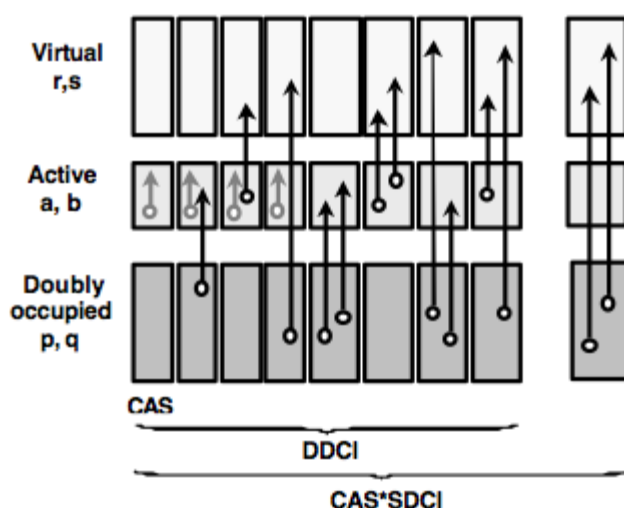


Fig. 12 Schematic representation of the CAS and DDCI space

There are three different formulations of DDCI. DDCI1 incorporates the CAS and all single excitations (1h, 1p or 1h1p). DDCI1 covers the first four columns of fig. 12. In line with Brillouin's theorem it is expected that the contribution of the single excited states is zero. This is due to the fact that the SCF procedure gives already the best linear combination of MOs. However the DDCI method is an uncontracted, entirely variational method meaning that the coefficients of the determinants in the CSFs do not necessarily stay the same and therefore can give a non-zero contribution. Nevertheless it is still expected that the DDCI1 wavefunction gives only a minor improvement.

DDCI2 incorporates besides the single excitations also all the double excitations towards or from the active space, these are on the one hand the configurations with two holes in the inactive space and two electrons extra in the CAS and on the other hand the configurations with two electrons in the virtual space and two electrons less in the CAS (2h, 2p). DDCI2 concerns the first six columns of fig. 12. The results of DDCI2 are normally very well for biradicals and dinuclear complexes but for ionic solids the obtained J values can deviate around 30% from the experimentally obtained values.²⁶

DDCI3 also includes all double excitations with one excitation from the inactive to virtual space together with one excitation from or towards the active space (2h1p, 1h2p). DDCI3 calculations are much more demanding than the DDCI2 calculations.²⁵

DDCI3 covers the whole CAS+SDCI space except the double excitations from the inactive to the virtual space (2h2p). These (2h2p)-double excitations are not included because they do not give any contribution to the off-diagonal elements:

$$\langle D_{pq,rs}^+ \Psi_I | \hat{H} | \Psi_J \rangle = 0 \quad \text{for } I \neq J \quad (12)$$

Here the D operator is a double excitation operator and Ψ_i and Ψ_j are two different CSFs.²⁴

The most important new contribution going from DDCI2 to DDCI3 is the effect of the ligand-to-metal charge transfer excitations. These excitations are already present in the DDCI2 space but the DDCI2-wavefunction has too less flexibility for taking into account significant orbital relaxation arising from these CT states.^{25,27}

Often DDCI gives excellent result; the most important disadvantage is that the number of CSFs that is taken into account increases very rapidly with increasing number of orbitals. The dimension of the DDCI3 calculation is proportional to $Dimension[CAS] * N_{orb}^3$. From table 2 it follows that the dimension of the CAS for a singlet state can be significantly higher than the dimension of a high spin state.

BASIS SETS & RELATIVITY

For the CASSCF, CASPT2 and DDCI calculations Atomic Natural Orbital basissets were used. These ANO basissets were obtained as the eigenfunctions of the average density matrices from CASSCF/CASPT2 wavefunctions.²⁸

There are small, large and relativistic variants of these basis sets, ANO-S, ANO-L and ANO-RCC respectively. When the ANO-RCC basis set is used, relativistic effects are included via the Douglas Kroll method. The most remarkable effect is the orbital-contraction/expansion effect. Due to relativity the s and p shells exhibit contraction and the d and f orbitals exhibit expansion. This can have an effect on the amount of orbital overlap and thus for the magnitude of the magnetic exchange interactions.

OTHER

CHOLESKY DECOMPOSITION

To store the two electron integrals the Cholesky decomposition is used. This is a method to store the two electron integrals efficiently saving memory. By using this decomposition more advanced calculations can be performed. The Cholesky decomposition uses the fact that a symmetric matrix A when it has positive eigenvalues can be factored into a product LL^T . Here L is a lower triangular matrix.²⁹

MAGNETIC COUPLING DETERMINATION

Magnetic interactions are mostly described in terms of magnetic couplings with symbol J . A magnetic coupling can be understood as the energy needed for an electron to flip the spin. Magnetic couplings are rationalized with the use of spin Hamiltonians. These Hamiltonians assume that the spatial part of the wavefunction stays the same for all different spin states and therefore the spin Hamiltonian takes into account only the spin part of the wavefunction. The most widely used spin Hamiltonians are the Heisenberg-Dirac-van Vleck (HDVV) Hamiltonian and the Ising Hamiltonian.²⁶

HDVV HAMILTONIAN

For the embedded cluster calculation the Heisenberg-Dirac-Van Vleck Hamiltonian is used.

$$\hat{\mathcal{H}}^{HDVV} = - \sum_{i,j=1}^N J_{ij} \hat{S}_i \cdot \hat{S}_j \quad (13)$$

For two magnetic centers this equation simplifies to

$$\hat{\mathcal{H}}^{HDVV} = -J \hat{S}_1 \cdot \hat{S}_2 \quad (14)$$

Or in an alternative form as:

$$\hat{\mathcal{H}}^{HDVV} = -\frac{1}{2}J(\hat{S}^2 - \hat{S}_1^2 - \hat{S}_2^2) \quad (15)$$

Where S^2 is:

$$S^2 = (\hat{S}_1 + \hat{S}_2)^2 = \hat{S}_1^2 + \hat{S}_2^2 + 2\hat{S}_1 \cdot \hat{S}_2 \quad (16)$$

The eigenvalues of the S^2 operator are $S(S+1)$ and so the eigenvalues of the Heisenberg Hamiltonian becomes:

$$E(S) = -\frac{1}{2}J(S(S+1) - S_1(S_1+1) - S_2(S_2+1)) \quad (17)$$

Because we are interested in energy differences we can drop the constant S_1 and S_2 terms. For the energy difference between two spin states with $\Delta S=1$ it can be derived easily that:

$$\Delta E = E(S-1) - E(S) = J * S \quad (18)$$

This is called the Landé interval rule.³⁰

Table 3 the number of J couplings between the spin state, S in respect to the lowest spin state, S=0

Spin, S	multiplicity	n*J
0	1	0
1	3	1
2	5	3
3	7	6
4	9	10
5	11	15

For the manganese containing crystals the singlet and undectet (11) states are investigated and the energy difference has to be divided by 15 to obtain the J coupling. For the iron containing crystals the singlet and nonet (9) are investigated and the energy differences have to be divided by 10 to obtain the J coupling.

The amount of J couplings between different spin states

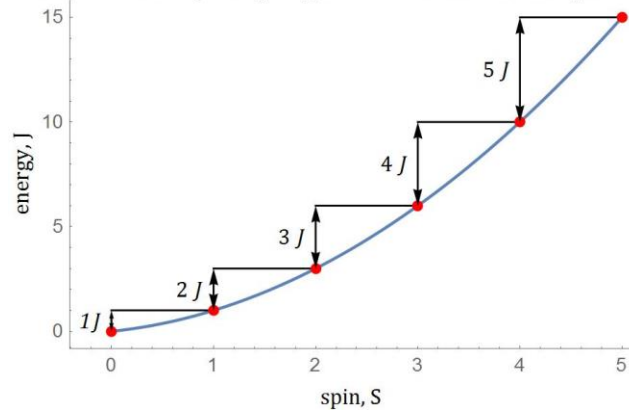


Fig. 13 Schematic plot of the energy versus the total spin. E=0 for S=0

It follows from table 3 that for higher spin systems fewer configurations are allowed, it is therefore computationally preferred to investigate the highest spin states and obtain the J coupling from the energy difference of these states. This is done for the DDCI calculations where it is computationally undoable to calculate the energies of the lowest spin states.

ISING HAMILTONIAN

The HDVV Hamiltonian can be rewritten in terms of the spin-ladder operators and the S_z component.³¹

$$\hat{S}^+ = \hat{S}_x + i\hat{S}_y \text{ and } \hat{S}^- = \hat{S}_x - i\hat{S}_y \quad (19)$$

$$\hat{H} = -\frac{1}{2}J (\hat{S}_1^+ \hat{S}_2^- + \hat{S}_1^- \hat{S}_2^+) - J\hat{S}_{z,1} \hat{S}_{z,2} \quad (20)$$

The Ising Hamiltonian is obtained by neglecting the ladder operator term and generalizing it to more than two spins.

$$\hat{H}^{Ising} = - \sum_{\langle i j \rangle}^n J_{ij} \hat{S}_{z,i} \cdot \hat{S}_{z,j} \quad (21)$$

Here $\langle i j \rangle$ indicates that they are nearest neighbors. The Ising Hamiltonian and the HDVV Hamiltonian do not commute, $[\hat{H}^{HDVV}, \hat{H}^{Ising}] \neq 0$, so they do not necessarily have a common set of eigenfunctions.

We use the Ising Hamiltonian for the periodic calculations. To keep things simple first a 1D chain is considered with a unit cell of two atoms.

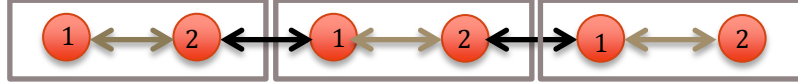


Fig. 14 Schematic representation of a one dimensional crystal with two atoms

The Ising Hamiltonian for one unit cell is:

$$\hat{H}^{Ising} = -J_{12} \hat{S}_{z1} \cdot \hat{S}_{z2} - J_{21} \hat{S}_{z2} \cdot \hat{S}_{z1} \quad (22)$$

And when atom 1 and atom 2 are chemically equivalent $J_{12}=J_{21}=J$.

$$\hat{H}_{cell}^{Ising} = -2J \hat{S}_{z1} \cdot \hat{S}_{z2} \quad (23)$$

The eigenvalues of the S_z operator are the spin magnetic moments m_s . When atom 1 and atom 2 are spin- $1/2$ particles the ferromagnetic and antiferromagnetic energies are:

$$E(FM) = -2J \left(\frac{1}{2}\right) \left(\frac{1}{2}\right) = -\frac{1}{2}J \quad (24)$$

$$E(AFM) = -2J \left(\frac{1}{2}\right) \left(-\frac{1}{2}\right) = \frac{1}{2}J$$

And the energy difference

$$\Delta E = E(AFM) - E(FM) = J \quad (25)$$

In this thesis we considered manganese and iron atoms that are not spin- $1/2$ particles but spin- $5/2$ and spin- $4/2$ particles respectively. In that case we obtain:

$$\Delta E = E(AFM, 5/2) - E(FM, 5/2) = 25J \quad (26)$$

$$\Delta E = E(AFM, 4/2) - E(FM, 4/2) = 16J$$

So here the energy differences are divided by the number of J to obtain the pure J factor.

For the OIH crystals two dimensions are considered. The unit cells of the crystals have two separate planes with magnetic centers: the (001) plane and the (002) plane. These planes are schematically represented below.

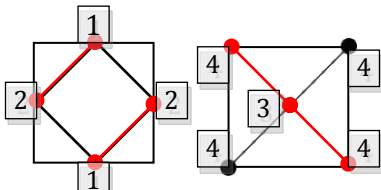


Fig. 15 Schematic representation of the two perovskite planes ((001) left and (002) right) in a single unit cell

First we assume that there are two different J-couplings. One in the [110] direction, $J^{(+)}$ and one in the $[\underline{1}10]$ direction, $J^{(-)}$. All the atoms are in a chemically equivalent position so $J_{12}^{(+)} = J_{21}^{(+)} = J_{34}^{(+)} = J_{43}^{(+)}$ and the same applies for $J^{(-)}$.

$$\begin{aligned} \hat{\mathcal{H}}^{Ising} = & -J_{12}^{(+)}(S_{z,1} \cdot S_{z,2} + S_{z,2} \cdot S_{z,1} + S_{z,3} \cdot S_{z,4} + S_{z,4} \cdot S_{z,3}) \\ & -J_{12}^{(-)}(S_{z,1} \cdot S_{z,2} + S_{z,2} \cdot S_{z,1} + S_{z,3} \cdot S_{z,4} + S_{z,4} \cdot S_{z,3}) \end{aligned} \quad (27)$$

So in both directions we get four separate J-couplings, making 8 couplings in total per unit cell. Considering manganese atoms all $S_i \cdot S_j$ terms become $\frac{5 \cdot 5}{2} = \frac{25}{4}$:

$$\begin{aligned} E\left(FM, S = \frac{5}{2}\right) &= -J_{12}^{(+)}\left(\frac{25}{4} + \frac{25}{4} + \frac{25}{4} + \frac{25}{4}\right) - J_{12}^{(-)}\left(\frac{25}{4} + \frac{25}{4} + \frac{25}{4} + \frac{25}{4}\right) \\ &= -J_{12}^{(+)}\left(\frac{100}{4}\right) - J_{12}^{(-)}\left(\frac{100}{4}\right) \\ &= -25J_{12}^{(+)} - 25J_{12}^{(-)} \end{aligned} \quad (28)$$

$$\begin{aligned} E\left(AMF, S = \frac{5}{2}\right) &= -J_{12}^{(+)}\left(-\frac{25}{4} - \frac{25}{4} - \frac{25}{4} - \frac{25}{4}\right) - J_{12}^{(-)}\left(-\frac{25}{4} - \frac{25}{4} - \frac{25}{4} - \frac{25}{4}\right) \\ &= -J_{12}^{(+)}\left(-\frac{100}{4}\right) - J_{12}^{(-)}\left(-\frac{100}{4}\right) \\ &= 25J_{12}^{(+)} + 25J_{12}^{(-)} \end{aligned} \quad (29)$$

$$\Delta E = E\left(AMF, S = \frac{5}{2}\right) - E\left(FM, S = \frac{5}{2}\right) = 50J_{12}^{(+)} + 50J_{12}^{(-)} = 100J_{12}^{(\pm)} \quad (30)$$

When we couple the spins ferromagnetically in the [110] direction and anti-ferromagnetically in the $[\underline{1}10]$ direction we need to double the cell in the [100] and [010] direction.

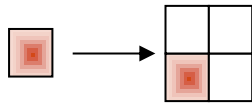


Fig. 16 Schematic representation of doubling the unit cell in the [010] and [100] direction

MAGNETIC EXCHANGE

The distances between the nearest magnetic metal centers in the hybrid crystals are around 5 Å. This distance is too large to have a significant direct exchange. Therefore the magnetization is bridged by the ligand. This process is called indirect exchange.³² The ligand that links the magnetic units together can be called a bridging ligand because it facilitates the electron delocalization of the magnetic units towards each other.³²

The ability of electrons to delocalize gives rise to an energy lowering, hence the state that causes the most delocalization will be the energetically favored state. The amount of delocalization depends much on the overlap between the magnetic units and the ligands.

In the superexchange mechanism the metal orbitals are bridged by a nonmagnetic orbital. Anderson, Goodenough and Slater formulated some rules to predict a ferromagnetic or antiferromagnetic interaction. For a d^5 - d^5 , as in the manganese hybrids they all predict an antiferromagnetic coupling and for a d^6 - d^6 , as in the iron based hybrids they also predict an antiferromagnetic coupling.³² In contrast a copper based hybrid, d^9 - d^9 couples ferromagnetically.³³

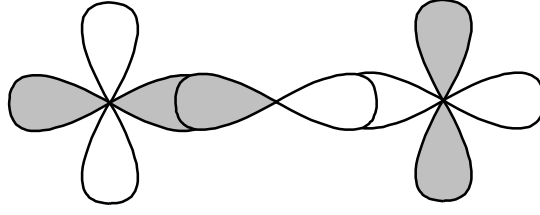


Fig. 17 Schematic representation of a 180 degree d-p-d superexchange antiferromagnetic situation

The principle of the exchange mechanism in our system is analogous to a simple system with two $S=1/2$ particles. We assume a system with two magnetic centers in two spatially localized singly occupied valence orbitals a and b . Also an inactive orbital localized on the bridging ligand is taken into account; called h . Orbital h is lower in energy and doubly occupied. It is outside the active space but facilitates the delocalization of the electrons.³⁴

First a CAS with orbitals a and b in two electrons is considered. In this situation the role of h is only implicit in the Fock operator. After the CASSCF mechanism is elaborated also the important role of the excitations from h to the CAS space are considered.

The four possible spin state configurations in the CAS with orbital a and b , two electrons and h doubly occupied are:

$$CAS(2,2) = \{ |h\bar{h}a\bar{b}|, |h\bar{h}b\bar{a}|, |h\bar{h}a\bar{a}|, |h\bar{h}b\bar{b}| \} \quad (31)$$

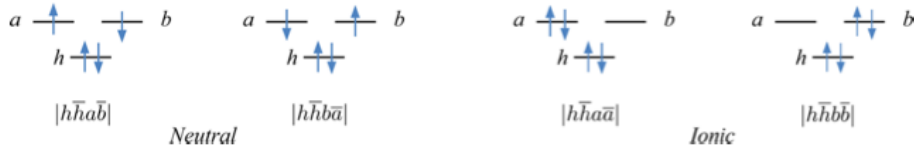


Fig. 18 A schematic representations of a CAS(2,2) and one core orbital h .³⁴

Setting $E=0$ for the neutral configurations a CI matrix can be written as:

$$CI = \begin{matrix} |h\bar{h}a\bar{b}| \\ |h\bar{h}b\bar{a}| \\ |h\bar{h}a\bar{a}| \\ |h\bar{h}b\bar{b}| \end{matrix} \begin{bmatrix} 0 & K_{ab} & t_{ab} & t_{ab} \\ K_{ab} & 0 & t_{ab} & t_{ab} \\ t_{ab} & t_{ab} & U & K_{ab} \\ t_{ab} & t_{ab} & K_{ab} & U \end{bmatrix} \quad (32)$$

K_{ab} is the exchange integral, U the energy of the ionic states and is positive and t_{ab} is the hopping integral:

$$t_{ab} = \langle a\bar{b} | \hat{H} | a\bar{a} \rangle = \langle a | \hat{F} | b \rangle \quad (33)$$

Diagonalization of the CI matrix gives one triplet and three singlet states. Finally the energy difference between the triplet and the lowest singlet state can be stated as:

$$\begin{aligned} \Delta E &= E(S_g) - E(T) \\ &= \left(K_{ab} + \frac{U - \sqrt{U^2 - 16t_{ab}^2}}{2} \right) - (-K_{ab}) \\ &= 2K_{ab} - \frac{4t_{ab}^2}{U} \end{aligned} \quad (34)$$

In the last step we assumed that the ionic state energy is much larger than the hopping integral. The first term is the direct exchange coupling between a and b , the second term is called the kinetic exchange. The first term favors ferromagnetic alignment. The second term favors an anti-ferromagnetic alignment.³⁴ One of the kinetic exchange pathways (there are four) is schematically represented in fig. 19.

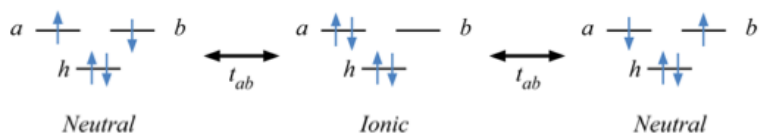


Fig. 19 Schematic representation of the kinetic spin exchange mechanism via the ionic state in a CAS(2,2) space.³⁴

Until now the role of the doubly occupied h orbital was only implicit. Now excitations from h to the CAS will also be considered. These excitations are considered explicitly in the DDCI1 calculations and called the 1h excitations. In our simple model all these 1h excitations are related to ligand-to-metal charge transfer excitations (LMCT). In the mechanism depicted in fig. 20 first a beta-electron is excited from the bridging h orbital to site a , followed by the beta electron in orbital b going to orbital h . In this way the ionic configuration is reached. After that the electron on h with opposite spin can go to orbital b followed by the electron on orbital a with the same spin going to h . In this way the system arrives at the exactly opposite situation. This mechanism is called superexchange and it is only possible when the spin in a and b are initially in an anti-ferromagnetic state and therefore favors an anti-ferromagnetic alignment. This mechanism effectively increases the t_{ab} term of the kinetic exchange term in equation 34.

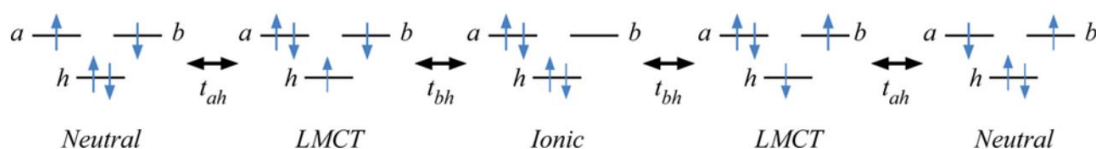


Fig. 20 Schematic representation of the superexchange mechanism.³⁴

Due to Brillouin's theorem the contributions of the 1h and 1p single excitations are small; therefore higher order mechanisms need to be included in the calculations to describe the J coupling appropriately.

The inclusion of the 1h-1p single excitations give rise to two kinds of effects. On the one hand the 1h-1p excitations that do not change the spin part cause an energy lowering of the ionic CAS configurations, the U term in equation 34. On the other hand there are the 1h-1p excitations that do change the spin. The spin change is compensated by another spin change in the CAS and therefore influence the direct exchange term, K_{ab} in equation 34.

Higher order 2h and 2p configurations in DDCI2 give rise to extra kinetic exchange effects favoring mostly the AFM state.³⁴ The 2h-1p and 1h-2p excitations that are included in DDCI3 give rise to multiple subtle effects which overall effect is an increase of the absolute J value.

RESULTS & DISCUSSION

ONE ATOM.

Before we look at the magnetic properties of the total crystal structure it is important to understand the magnetic centers itself. Calculations are performed on a single manganese or iron atom and on a MCl_6 octahedral molecule. In this way we get insight in how the various methods perform in respect to each other. For the MCl_6 the geometry is taken from the MNMA and FEMA crystals.



Fig. 21 A MCl_6^{4-} molecule, with M is Mn or Fe.

For one manganese atom in a spherical environment the possible term symbols in a d^5 configuration are: 6S , 4G , 4F , 4D , 4P , 2I , 2H , $2\cdot{}^2G$, $2\cdot{}^2F$, $3\cdot{}^2D$, 2P and 2S . According to the first Hund's rule the state with maximum spin, 6S , is the ground state.

We perform CASSCF, CASPT2 and DDCI calculations on the sextet, lowest quartet and lowest doublet state of a bare Mn^{2+} ion and a Mn^{2+} ion with six Cl^- ions in octahedral environment.

ANO-L-VTZp is used as a basis set and an active space is defined as the five 3d orbitals with 5 electrons (CAS(5,5)). The high spin state with α spin in all 5d orbitals gives a sextet state with only one possible configuration. The other possible multiplicities are the doublet and quartet states with 100 and 25 possible configurations respectively.

In the two tables below the CASSCF, CASPT2 and DDCI1-3 energies and two energy differences are given. The first one is the energy difference between the sextet and the quartet state and the second one is the energy difference between the sextet and the doublet state.

Table 4 The energy differences between sextet, quartet and doublet states calculated with CASSCF and CASPT2

ANO-L-VTZp	mult	CASSCF		CASPT2	
		E (a.u)	ΔE (a.u.)	E (a.u.)	ΔE (a.u.)
octahedral $Mn_1Cl_6^{4-}$	6	-3906,835		-3908,465	
	4	-3906,711	0,124	-3908,355	0,111
	2	-3906,658	0,177	-3908,305	0,160
spherical Mn^{2+}	6	-1149,106		-1149,416	
	4	-1148,961	0,145	-1149,286	0,130
	2	-1148,898	0,208	-1149,227	0,189

Table 5 The energy differences between sextet, quartet and doublet states calculated via DDCI

ANO-L-VTZ	mult	DDCI1		DDCI2		DDCI3	
		E(a.u)	ΔE (a.u.)	E (a.u.)	ΔE (a.u.)	E (a.u.)	ΔE (a.u.)
octahedral $Mn_1Cl_6^{4-}$	6	-3906,834		-3906,896		-3907,000	
	4	-3906,717	0,117	-3906,790	0,106	-3906,900	0,100
	2	-3906,665	0,169	-3906,741	0,155	-3906,855	0,145
spherical Mn^{2+}	6	-1149,107		-1149,168		-1149,229	
	4	-1148,963	0,145	-1149,026	0,142	-1149,087	0,142
	2	-1148,899	0,208	-1148,957	0,211	-1149,019	0,210

As one can see the energy difference between the different multiplicities is around 0,1-0,15 a.u. for ΔE^{4-6} and around 0,15-0,21a.u. for ΔE^{2-6} . The energy gap between the sextet and quartet state is larger than the energy gap between the doublet and quartet state.

Compared to magnetic couplings later on in this project these energy differences are very large. As a result the ground state of the Mn^{2+} ion will always be the sextet, 6S state. This fact also allows us to use the HDVV Hamiltonian because it assumes that the separation of the electronic states is much larger than the states caused by the magnetic interaction.

Of course the absolute CASPT2 energies are lower than the CASSCF energies because CASPT2 recovers more correlation energy. However the CASSCF energy differences are larger than the CASPT2 energy differences. This is also expected; for the high spin state only one configuration is taken into account while for the $S=4$ and $S=2$ there are several configurations to take into account. The more configurations the larger the correlation energy, so the energy lowering increases for lower multiplicities. Because the sextet energy is the lowest state, the energies come closer together by including more correlation energy.

The energy differences are larger for the bare manganese cation than for the $MnCl_6$ system. This can be explained by the fact that the spin on the $MnCl_6$ system is more delocalized on the chlorine atoms resulting in an energy lowering.

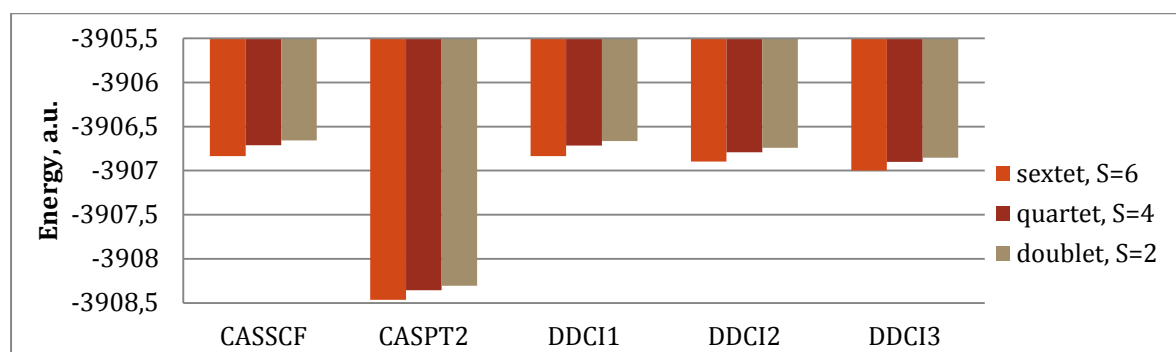


Fig. 22 CASSCF, CASPT2, and the DDCI1,2,3 energies of $MnCl_6^+$ in the lowest doublet, quartet and sextet state.

From the diagram above concerning the energies of the octahedral complex it can be easily seen that the CASPT2 method recovers much more dynamic correlation in contrast to the DDCI results. This emphasizes that the DDCI is focused on energy differences. In this particular case the CASSCF and the DDCI1 are practically the same. This is also expected in accordance to Brillouin's theorem.

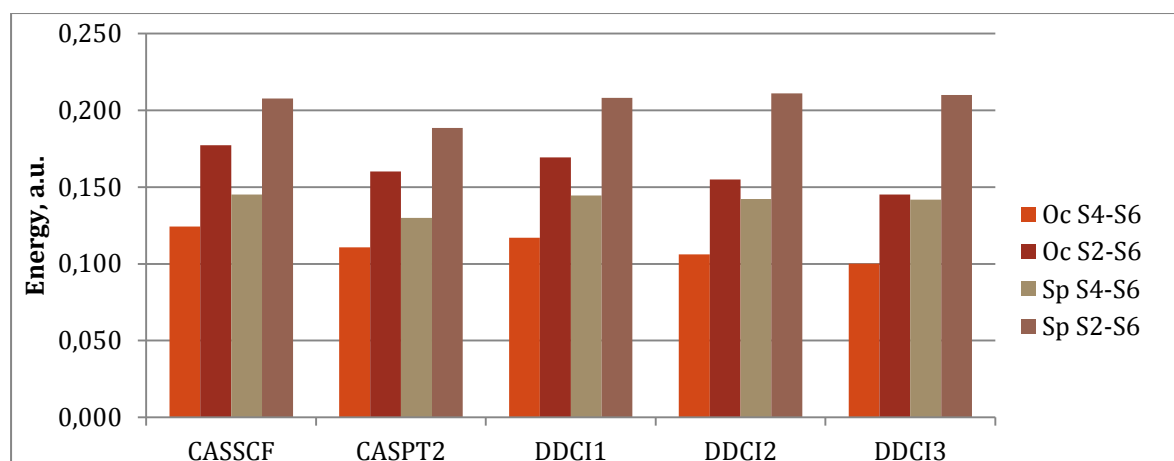


Fig. 23 Energy differences of the octahedral(Oc) MnCl_6^{4-} molecule and the spherical(Sp) Mn^{2+} cation.

Focusing instead on the energy differences it is notable that the different methods give very similar results. For the octahedral system the CASSCF overestimates the energy difference. For the octahedral system the energy differences decrease by going from DDCI1 to DDCI2 to DDCI3. This trend is also expected for the same reason as described above between CASSCF/CASPT2, namely that for the lower multiplicities more correlation energy is covered.

Similar calculations are performed on a Fe^{2+} cation and a FeCl_6^{4-} system. Fe^{2+} has a d^6 configuration. The lowest energy term symbol is 5D , quintet state. The energies of the quintet, lowest triplet and lowest singlet states are calculated and presented below.

Table 6 Energy differences between quintet, triplet and singlet states calculated with CASSCF and CASPT2

ANO-L-VTZp	CASSCF			CASPT2	
	mult	E (a.u.)	ΔE (a.u.)	E (a.u.)	ΔE (a.u.)
octahedral $\text{Fe}_1\text{Cl}_6^{4-}$	5	-4019,393		-4021,099	
	3	-4019,310	0,083	-4021,022	0,078
	1	-4019,282	0,111	-4020,990	0,110
spherical Fe^{2+}	5	-1261,658		-1262,030	
	3	-1261,553	0,104	-1261,936	0,094
	1	-1261,504	0,154	-1261,880	0,150

Table 7 Energy differences between quintet, triplet and singlet states calculated with DDCI

ANO-L-VTZ	Mult	DDCI1		DDCI2		DDCI3	
		E (a.u.)	ΔE (a.u.)	E (a.u.)	ΔE (a.u.)	E (a.u.)	ΔE (a.u.)
spherical Fe^{2+}	5	-1261,708		-1261,937		-1261,887	
	3	-1261,647	0,061	-1261,832	0,105	-1261,778	0,108
	1	-1261,602	0,106	-1261,784	0,153	-1261,731	0,156

Analogous to the manganese case the energy differences of the octahedral FeCl_6^{4-} are smaller. Also the CASPT2 energy differences are smaller although the difference is less pronounced.

The magnetic couplings of the bare iron cation are larger than the couplings of the octahedral FeCl_6 . Also here it can be explained by the energy lowering caused by delocalization to the chlorine anions.

The energies of the spherical Fe^{2+} are all close each other. The energy differences are close together when CASSCF, CASPT2 and DDCI2 and DDCI3 are compared with each other (approximately 0,10 a.u. and 0,15 a.u.) while the DDCI1 results are a bit lower (0,061 a.u. and 0,106 a.u.).

PERIODIC CALCULATIONS.

The positions of the hydrogen atoms were optimized with DFT/PBE using CRYSTAL. Afterwards the Ising couplings were determined. The perovskite layers are parallel to the *ab* planes, but the Mn-Cl-Mn chains are not parallel to the *a* and *b* axis but parallel to the [110] axis, and the $[\bar{1}10]$ axis.

For the in-plane coupling the spins have an exchange interaction in the [110] and the $[\bar{1}10]$ direction. These directions are not identical because the buckling angle is only present in one of these directions. To investigate the couplings in the direction with, or without a buckling angle the magnetic unit cells had to be doubled. For this reason a {221} supercell was made. This means that the unit cell is doubled in the *a* and *b* direction. The resulting unit cell is four times as large as the original one. The supercell allows for coupling the spins ferromagnetically in the [110] direction and anti-ferromagnetically in the $[\bar{1}10]$ directions and vice versa. In fig. 24 the different coupling schemes are shown.

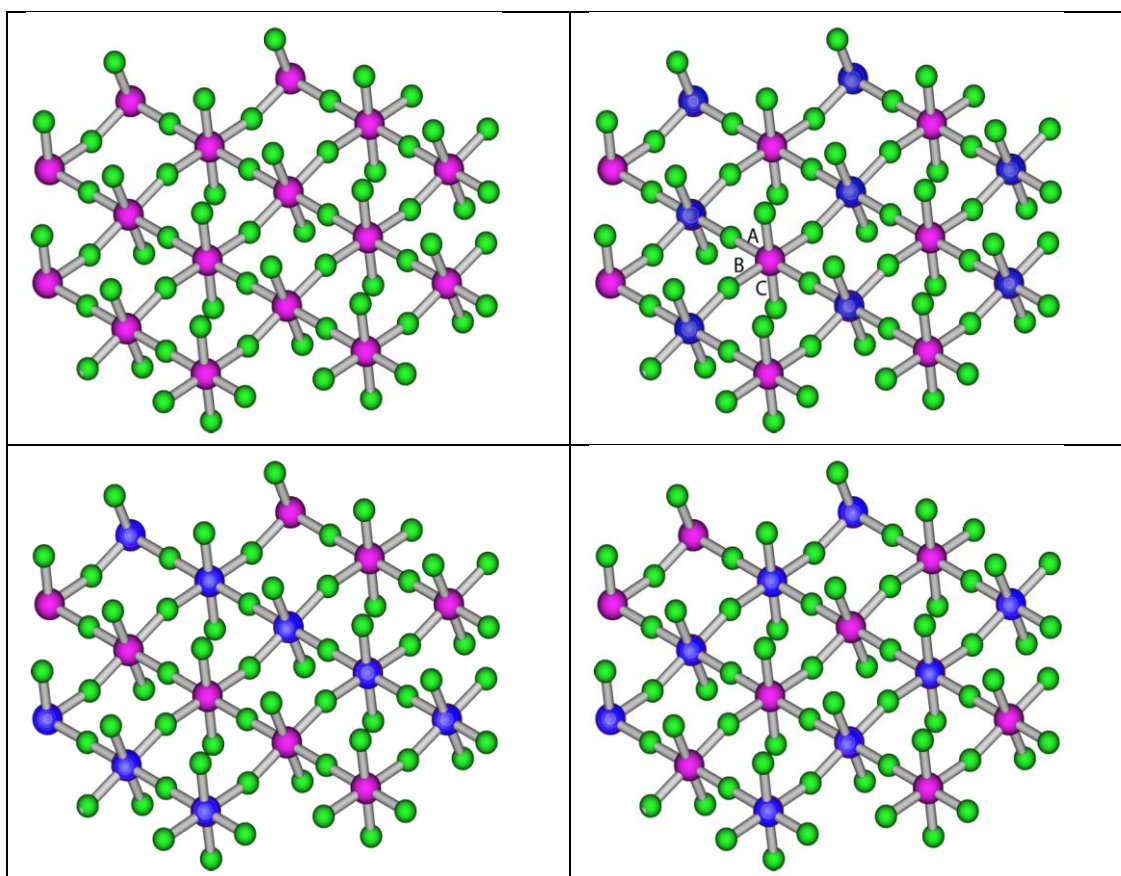


Fig. 24 Different coupling schemes; blue and purple represent manganese cations with α or β spin. The green atoms are chlorine. top-left: ferromagnetic, top-right: anti-ferromagnetic, bottom-left: FM/AFM and bottom-right: AFM/FM

In the following tables the energies are given for the different coupling schemes. The first column indicates ferromagnetic (F) and antiferromagnetic (A) coupling in the 110/1 $\bar{1}0$ (/001) direction respectively. The “n*J” column gives the number of relevant interactions in one unit cell.

	total energy (a.u.)	ΔE (a.u.)	ΔE (eV)	n cells	n J/cell	$J_{25/2}$ (eV)	J (meV)
FFF	-5,0937290E+04	-	-	4	4	-	-
AF	-5,0937312E+04	-2,25E-02	-0,61	4	4	-0,0382	-3,05
FA	-5,0937312E+04	-2,25E-02	-0,61	4	4	-0,0382	-3,05
AA	-5,0937333E+04	-4,31E-02	-1,17	4	8	-0,0367	-2,93
FFA	-5,0937290E+04	-4,4E-06	-1,20E-04	4	NA	-3,0E-05	-2,4E-03

The total energy difference is divided by the number of unit cells and the number of Mn-Mn couplings that are present in one unit cell. The J coupling in the [110] and [$\bar{1}10$] directions are practically the same giving in both direction a J coupling of -3 meV. For the total AFM state however the J coupling is lower. This can be due to the fact that coupling in both direction influences each other. The inter layer coupling is anti-ferromagnetically and around -2 μ eV. However this J coupling is so small that it is probably below the accuracy range of the program.

To get an idea about the electronic structure a band structure diagram is calculated for this crystal. The top of the valence band, which is also the point of the Fermi energy is at -0,186 a.u. and the bottom of the conduction/virtual band is -0,098 a.u.

The resulting band structure diagram has an almost flat valence and conduction band and the energy gap is approximately 0,1 a.u. As a conclusion the MNMA crystal does not have a low lying conducting state. This is also expected because neither the organic nor inorganic part consists of conducting moieties.

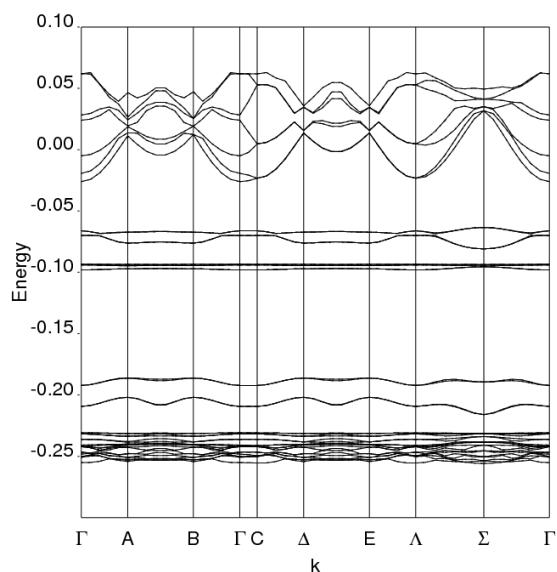


Fig. 25 Band diagram of MNMA: the Fermi level is at -0,186 a.u.

EMBEDDED CLUSTER CONSTRUCTION

After optimizing the hydrogen positions the clusters can be made. Therefore we need the Madelung fields and AIMP. To make the AIMP a large sphere with a radius of approximately 40 a.u. was constructed as illustrated in fig. 26. Then a Madelung field was created to surround the sphere. Then the SCEI procedure was used to make an AIMP for manganese and for chlorine. (see appendix B)

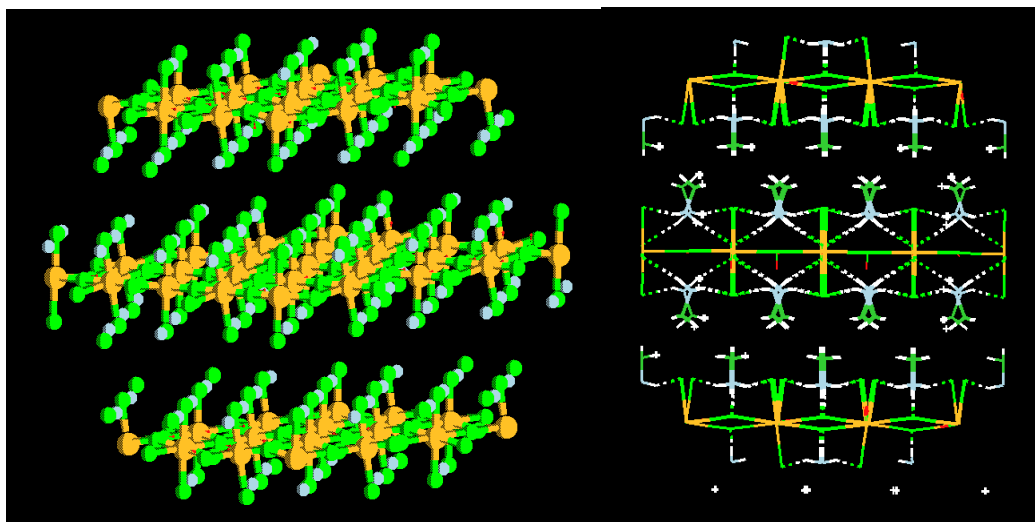


Fig. 26 Two representations of the large molecular sphere

After AIMP were implemented in the MOLCAS basis set library, a set of clusters were constructed. All clusters have two magnetic manganese centers and have as nearest neighbors six chlorine atoms. To each in-plane chlorine atom a Mn-AIMP was placed. In fig. 27 each manganese atom that is only attached to one chlorine atom is treated as an AIMP.

Clusters 3, 4 and 8 have only manganese and chlorine atoms while clusters 6, 7 and 9 have also included the four nearest ligands. Clusters 3 and 6 have a buckling angle perpendicular to the central Mn-Mn bond while clusters 4 and 7 have a buckling angle aligned with the central Mn-Mn bond.

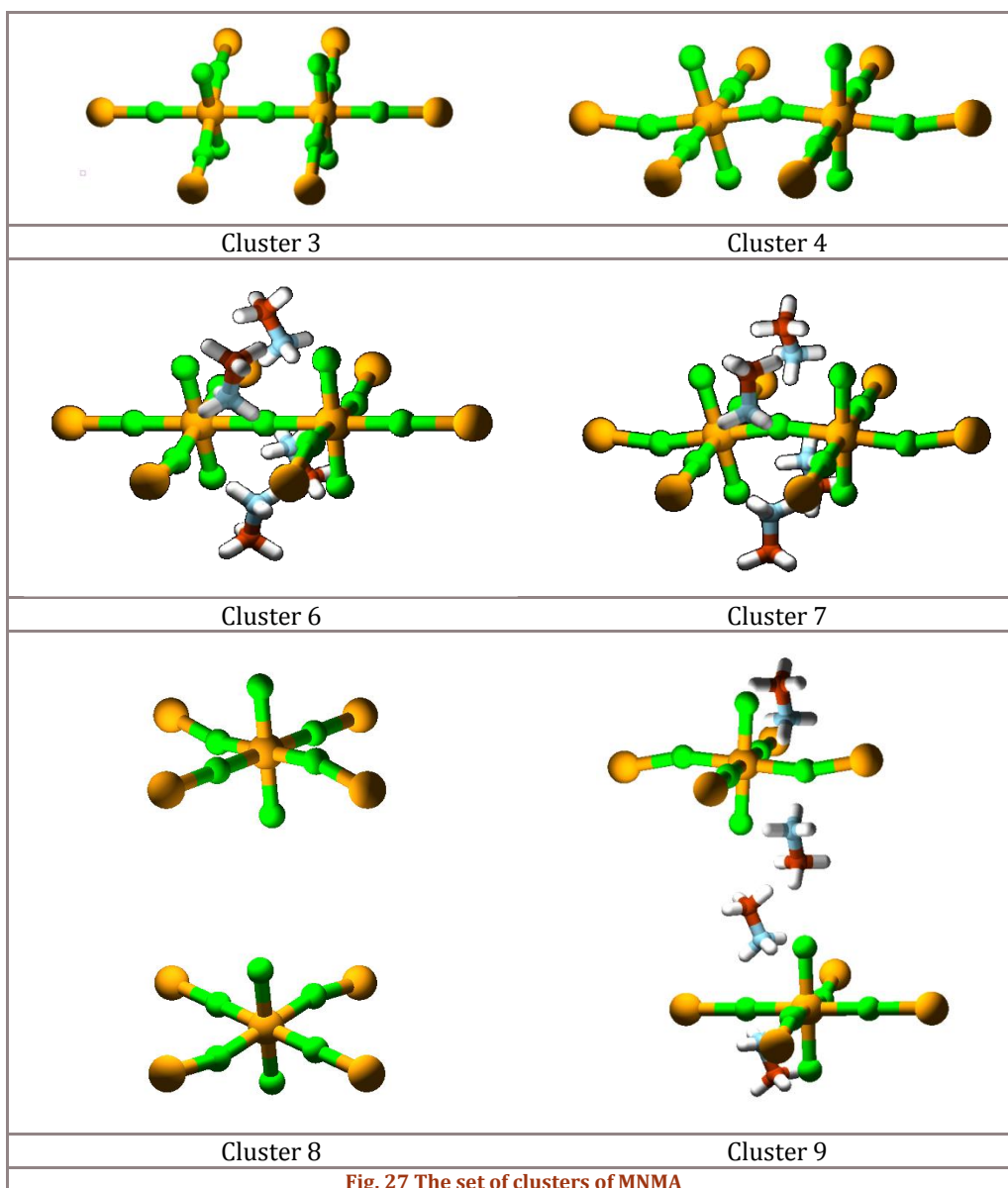


Fig. 27 The set of clusters of MNMA

Once the clusters were created for each cluster the Madelung fields are fitted with a radius between 30-45a.u. This gave for each crystal a set of a few hundred point charges that is included in the calculations.

To illustrate the whole embedded cluster, in fig. 28 cluster 4 is plotted with the Mn^{AIMP} 's indicated in purple and the small dots around the cluster are the positions of the point charges that form the Madelung field.

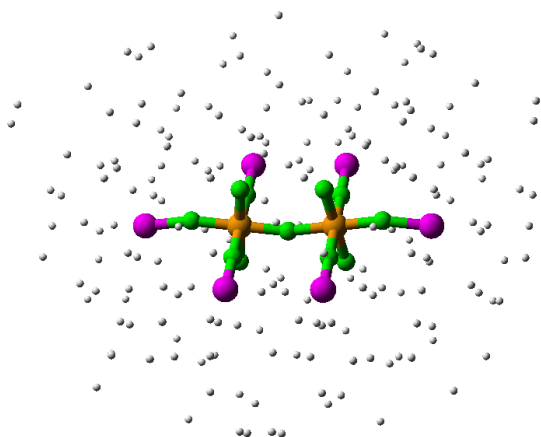


Fig. 28 The cluster with the AIMP's and the point charges

VALIDATION OF THE CLUSTER

To validate that the embedded cluster represents the original crystal appropriately, the same type of calculation as the periodic calculation is performed using the same method (DFT), functional (PBE) and basissets (Crystal basis set library). Cluster 4 is used to test the agreement.

In the table below the J value of the periodic calculation is obtained by equation 25. The embedded cluster calculation is performed using UDFT. The singlet state is forced to converge in the state where one manganese atom has all 3d orbitals singly occupied with α -electrons and the other manganese atom has all 3d orbitals singly occupied with β -electrons.

Table 8 Comparison of the embedded cluster model and the periodic calculation

total energy(a.u.)	ΔE (a.u.)	$\Delta E(eV)$	ncells	n^*J	$J_{(25/2)}$	$J(meV)$
periodic:						
FM: -5,09373E+04						
AFM: -5,09373E+04	-2,25E-02	-0,61	4	4	-0,0382	-3,05
embedded cluster:						
S1: -7369,727482						
S11: -7369,728901	-0,001419	-0,04	NA	1	-0,0386	-3,06

It can be seen that the agreement between the periodic cluster calculation and the embedded cluster calculation is very well.

Now the embedded cluster approach is validated more advanced MCSCF methods can be applied. In addition the ANO basis sets are used instead of the basis sets from the CRYSTAL library.

Firstly it is checked how much the energies depend on the size of the basis set and contraction. The various ANO basis sets are compared with each other. For the VTZ and VQZ basis sets in this thesis always the 3d orbitals on the chlorine atoms are included. This is why VTZ and VQZ are indicated as VTZ(p) and VQZ(p) in Table 9. The inclusion of the d orbitals on the chlorine atom gives the atom the ability to polarize towards the metal atoms.

Table 9 Number and type of basisfunctions of the ANO basissets for Manganese and Chlorine

ANO-L/RCC-...	Manganese	Chlorine
-MB	4s3p1d	3s2p
-VDZ	5s4p2d	4s3p
-VDZp	5s4p2d1f	4s3p1d
-VTZ(p)	6s5p3d	5s4p2d
-VTZp	6s5p3d2f1g	5s4p2d1f
-VQZ(p)	7s6p4d	6s5p3d

Because the calculations need a lot of memory for the two-electron integrals we apply the Cholesky decomposition and look for impact on the results. For convenience here only the energy differences are given in atomic units. To obtain the J coupling one has to divide the energy differences by $\frac{25}{2}$, however this is unnecessary when one wants to compare basisset effects of similar systems.

Table 10 Energy differences for cluster 4 for different ANO-L basissets

Basisset	Mult.	Energy(a.u.)	ΔE (a.u.)	Energy(a.u.)	ΔE (a.u.)
<u>ANO-L-...</u>		No Cholesky		Cholesky	
-MB	11	-7362,258301		-7362,253417	
	1	-7362,258553	-2,52E-04	-7362,253674	-2,57E-04
-VDZ	11	-7362,649841		-7362,646639	
	1	-7362,649982	-1,41E-04	-7362,646780	-1,41E-04
-VDZp	11	-7362,680145		-7362,678705	
	1	-7362,680313	-1,67E-04	-7362,678873	-1,68E-04
-VTZ (p)	11	-		-7362,765795	
	1	-	-	-7362,765964	-1,69E-04
-VTZp	11	-		-7362,777615	
	1	-	-	-7362,777784	-1,69E-04
-VQZ (p)	11	-		-7362,814836	
	1	-	-	-7362,815004	-1,69E-04

Also the effect of relativity is taken into account using the Douglass Kroll Hamiltonian and the relativistic ANO-RCC basis sets.

Table 11 Energy differences of cluster 4 for different ANO-RCC basissets

Basisset	Mult.	Energy(a.u.)	ΔE (a.u.)	Energy(a.u.)	ΔE (a.u.)
ANO-RCC-...		No Cholesky		Cholesky	
-MB	11	-7392,856311		-7392,851388	
	1	-7392,856495	-1,84E-04	-7392,851576	-1,87E-04
-VDZ	11	-7393,167484		-7393,163869	
	1	-7393,167634	-1,49E-04	-7393,164019	-1,50E-04
-VDZp	11	-7393,196539		-7393,194430	
	1	-7393,196719	-1,80E-04	-7393,194611	-1,81E-04
-VTZ (p)	11	-		-7393,283423	
	1	-	-	-7393,283594	-1,71E-04
-VTZp	11	-		-7393,294225	
	1	-	-	-7393,294395	-1,71E-04
-VQZ (p)	11	-		-7393,312048	
	1	-	-	-7393,312218	-1,70E-04

Without Cholesky decomposition there was not enough memory for the calculation with triple and quadruple zeta basis sets. This emphasizes the usefulness of the decomposition.

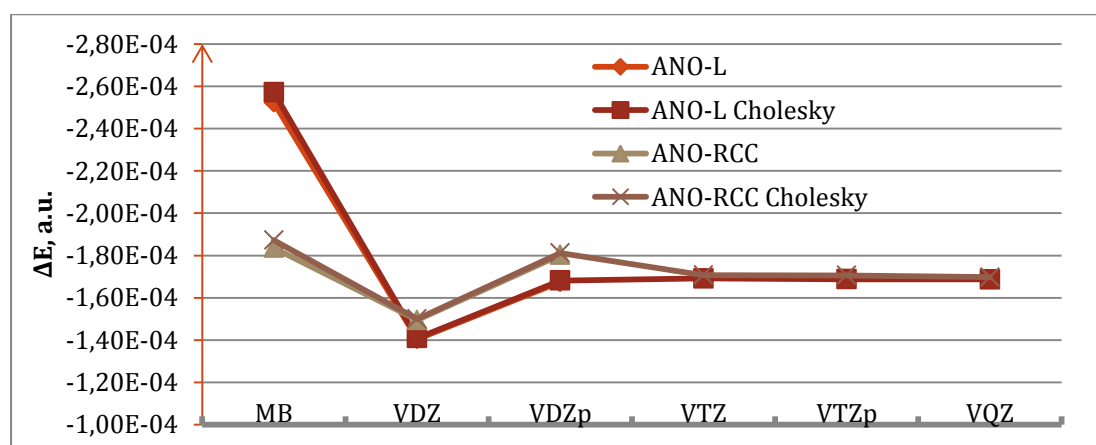


Fig. 29 ΔE for increasing basis-sets

Note that the vertical energy axis is inverted because the energy difference is negative indicating that the anti-ferromagnetic state is the lowest energy state.

The minimal basis (MB) overestimates the coupling while the VDZ clearly underestimates the magnetic coupling. Especially the non-relativistic minimal basis (ANO-L-MB) gives a large overestimation while larger basissets give an underestimation compared to the RCC ones. The VDZp basisset is more than 5% off from the VQZ energy. The VTZ, VTZp and VQZ are very close to each other so VTZ and VTZp are preferred. Hence the VTZ and VTZp basissets are chosen for the following calculations.

The effect of the Cholesky decomposition is not negligible for the absolute energies because they are around 0,002-0,005 a.u. higher in energy. However the Cholesky decomposition does not have any significant effect on the energy differences. For this reason we regard it as justified to use the Cholesky decomposition.

DECONSTRUCTION

Although removal of the Madelung field and the AIMPs presents a non-realistic system it is interesting to see how much impact the embedding has on the magnetic coupling. The following situations are studied for clusters 3 and 4:

- The full embedding original situation
- Replacing the bridging Cl with a point charge (PC) to break the indirect exchange mechanism (see fig. 30)

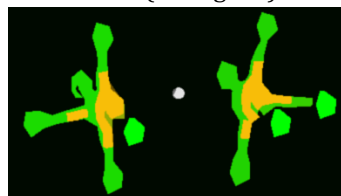


Fig. 30 Cluster with the central chlorine atom replaced by a point charge

- Removing the Madelung field but keeping the AIMPs
- Removing the AIMPs and the Madelung field
- Removing the chlorine atoms except the central one, the AIMPs and the Madelung field. (See fig. 31)

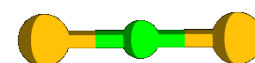


Fig. 31 Mn₂Cl system

Table 12 Energy differences for several variations on clusters 3 and 4

CASSCF/ANO-L-VTZp	mult	cluster 3		cluster 4	
		E (a.u.)	ΔE (a.u.)	E (a.u.)	ΔE (a.u.)
full embedding Mn ₂ Cl ₁₁ Mn ^{AIMP} ₆	11	-7362,774092		-7362,780317	
	1	-7362,774237	-1,45E-04	-7362,780486	-1,69E-04
Bridging Cl = PC Mn ₂ Cl ₁₀ Mn ^{AIMP} ₆	11	-6903,359064		-6903,813394	
	1	-6903,359064	-4E-08	-6903,813394	1,7E-07
no PCs Mn ₂ Cl ₁₁ Mn ^{AIMP} ₆	11	-7357,086655		-7357,088654	
	1	-7357,086802	-1,46E-04	-7357,088823	-1,70E-04
no PCs and no AIMPs Mn ₂ Cl ₁₁	11	-7353,500097		-7353,501037	
	1	-7353,500226	-1,29E-04	-7353,501184	-1,47E-04
no PCs/AIMPs and one Cl Mn ₂ Cl	11	-2758,192398		-2758,187833	
	1	-2758,192385	1,31E-05	-2758,187818	1,48E-05
no PCs/AIMPs and no Cl Mn ₂	11	-2297,798517		-2297,797578	
	1	-2297,798516	8,10E-07	-2297,797577	8,2E-07

The replacement of the central chlorine atom by a point charge decreases the magnetic interaction almost to zero. This is because there is no orbital overlap anymore as depicted in fig. 17 and there is not any possibility for indirect exchange anymore. For this reason the magnetic manganese centers do not 'feel' each other anymore and the anti-ferromagnetic alignment does not cause significant stabilization.³⁵

It follows from the results with no Madelung field (the no-PCs result) that the effect of the Madelung field on the magnetic coupling is small in the order of 1.E-6. This is also an indication that the magnetism in these crystals is a property that only depends on the local environment. This is a good argument to justify the embedded cluster approach.

The removal of the Madelung field and also the AIMPs gives a significant underestimation of the magnetic coupling of more than 10%. When the AIMPs are removed the electron density delocalizes too far away from the center. This causes a weaker interaction and therefore an energy lowering.

When besides the AIMPs and the Madelung field also the surrounding chlorine atoms are removed except the bridging chlorine atom, the coupling is decreased strongly and becomes

positive. This is clearly an unrealistic situation hence the effect of the neighbors is very important.

The results for clusters 3 and 4 follow the same trend but the energy differences of cluster 4 are somewhat higher. This is the cluster with the buckling angle, so the angle does increase the magnetic coupling a bit. The effect is however small.

A CLOSER LOOK AT CASSCF & CASPT2

CASSCF & CASPT2 calculations were performed on all clusters with the ANO-L-VTZp, ANO-L-VTZ and ANO-RCC-VTZ basissets:

Table 13 CASSCF J couplings of the MNMA clusters

CASSCF(10,10)	ANO-L-VTZp	ANO-L-VTZ	ANO-RCC-VTZ
	J (meV)	J (meV)	J(meV)
cluster 3	-0,264	-0,264	-0,267
cluster 6	-0,268	-0,269	-0,272
cluster 4	-0,306	-0,306	-0,309
cluster 7	-	-0,311	-0,313
cluster 8	0	0	0
cluster 9	0	0	0

Table 14 CASPT2 J couplings of the MNMA clusters

CASPT2(10,10)	ANO-L-VTZp	ANO-L-VTZ	ANO-RCC-VTZ
	J (meV)	J (meV)	J(meV)
cluster 3	-7,484	-6,127	-7,564
cluster 6	-5,826	-6,206	-6,245
cluster 4	-7,582	-7,564	-6,249
cluster 7	-	-6,291	-6,269
cluster 8	-	-2,151	-2,028
cluster 9	-	-0,829	-0,800

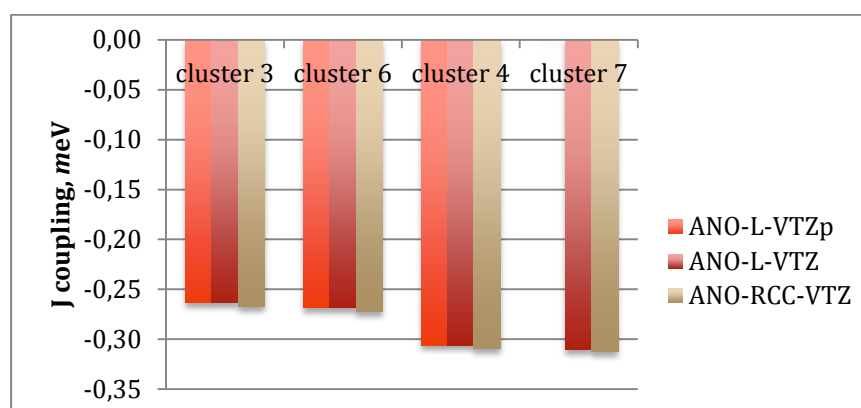


Fig. 32 J couplings per cluster CASSCF

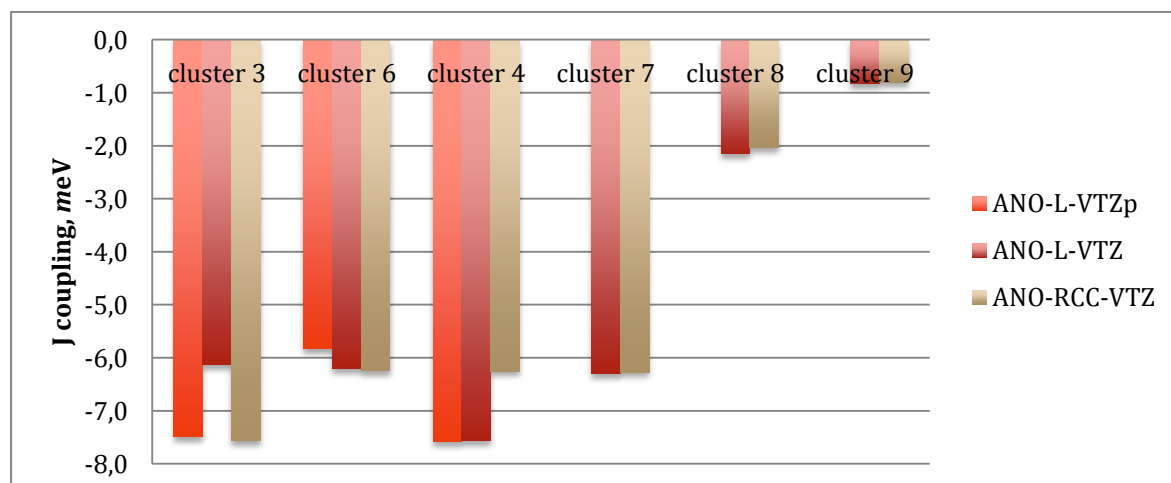
From the diagram it can be concluded that the inclusion of the methylamine ligands has very little effect on the intra-layer magnetic couplings, only $0,2 \cdot 10^{-5}$ a.u. ($0,05$ meV). The couplings from clusters 3 and 6 are almost the same and also the coupling of clusters 4 and 7 are almost the same. From the spin densities in table 15 it can be concluded that there is not any spin density found on the nitrogen atoms while there is spin density on the chlorine atoms so there is practically no exchange coupling via the nitrogen atom.

Table 15 Spin densities of cluster 6, CASSCF, S=11

Spin Densities	Mn	Bridging Cl	Cl	Cl _⊥	N
Cluster 6	4,916	0,025	0,016	0,014	0,000

The VTZ and VTZp results give the same answer for the CASSCF energies. So the VTZ basis set is large enough and a more extensive basis set does not give significant improvements. The clusters 3 and 6 have a straight central Mn-Cl-Mn bond while clusters 4 and 7 do not. The energy differences of buckled interactions are a bit stronger although the difference is small. The design of hybrid materials with a high as possible buckling angle will probably have rather small effects. Probably the orbital overlap increases when the buckling angle is increased causing a more efficient indirect exchange. (It would be interesting to see how the coupling depends on the Mn-Cl-Mn angle because for an angle of 90° a positive ferromagnetic J coupling is expected.)

Including relativistic effects gives a small increase in the energy difference. Relativity causes larger d orbitals giving larger interaction with the chlorine atom. This gives a little more efficient delocalization for the anti-ferromagnetic state.

**Fig. 33 J couplings per cluster CASPT2**

The CASPT2 results are more ambiguous than the CASSCF results. The first remarkable thing is that the energy differences are approximately 20 times larger. Because CASPT2 takes more correlation energy into account a significant energy difference is expected. This is because the singlet state contains more correlation energy than the high spin state. Nevertheless it was not expected that the CASPT2 energies were 20 times as large.

Unfortunately we cannot make any clear conclusion regarding the effect caused by the different basis sets from these calculations. Possibly some calculation did not converge to the correct state or there were some effects from intruder state. Also other studies showed that CASPT2 causes problems with high spin-weak magnetic coupling systems.³⁶ These problems are however not observed in DDCI calculations. Another possibility when DDCI is not feasible is the *n*-electron valence state-PT2 (NEVPT2) method, this method suffers less from intruder states but is cheaper than DDCI.³⁶ However this method is not implemented in MOLCAS, but gave already very good result in comparison with DDCI.^{36,34}

In any case the magnetic couplings calculated with CASPT2 are much larger than the couplings calculated via CASSCF, going from around -0,3 meV to around 8 meV. With CASPT2 also the inter layer clusters 8 and cluster 9 show a significant magnetic coupling of -2 and -1 meV respectively. It is much larger than expected, especially for cluster 8. For this reason we regard these results as unrealistic.

ALL MULTIPLICITIES

Because of the fact that a large CAS (10,10) has to be chosen the DDCI calculation of the low spin multiplicities are extremely large. And the low spin states are unmanageable to calculate.

To have still an idea about the J coupling we will investigate the possibility to only calculate the two highest spin states to obtain the J-coupling. To see that this works it is first applied to the CASSCF and CASPT2 methods. All possible multiplicities of cluster 3 are calculated. Then we calculate the J coupling in three different ways. In the first place we use the method that is applied throughout this whole project looking at the energy difference between the lowest and highest spin state and dividing it by the number of J couplings that it represents. Secondly we determine the J coupling by the energy difference of the two highest multiplicities, in this case 9 and 11. As a third method we fit all the energies to the line $\frac{1}{2}J(S(S+1))+c$ and obtain a value for J.

Table 16 Energy and ΔE vs multiplicity of cluster 3

ANO-RCC-VTZ	CASSCF		CASPT2	
multiplicity	E (a.u.)	ΔE (a.u.)	E (a.u.)	ΔE (a.u.)
11	-7393,28342	0,00E+00	-7395,65125	0,00E+00
9	-7393,28347	-5,01E-05	-7395,652191	-9,42E-04
7	-7393,28352	-9,51E-05	-7395,653029	-1,78E-03
5	-7393,28355	-1,32E-04	-7395,653734	-2,48E-03
3	-7393,28358	-1,57E-04	-7395,654297	-3,05E-03
1	-7393,28359	-1,71E-04	-7395,654699	-3,45E-03

The energies are plotted versus the multiplicity setting the singlet state as $E=0$.

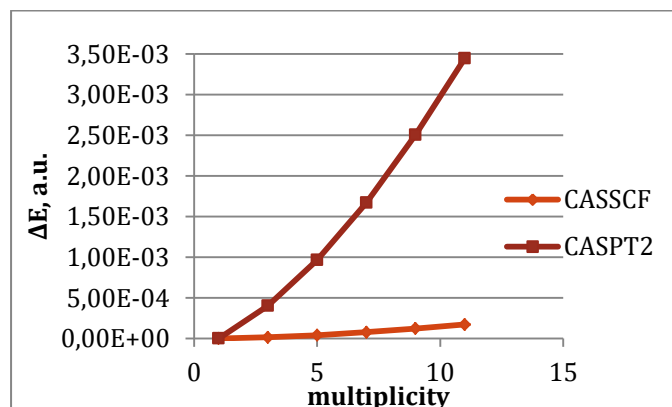


Fig. 34 ΔE versus spin multiplicity

From fig. 34 one can see the large difference between the CASSCF and CASPT2 methods.

We investigated how well the data fits to the $E=\frac{1}{2} \cdot J \cdot S(S+1)$ function and then obtain an average J coupling. Below the plots are given with ΔE (a.u.) versus spin, S.

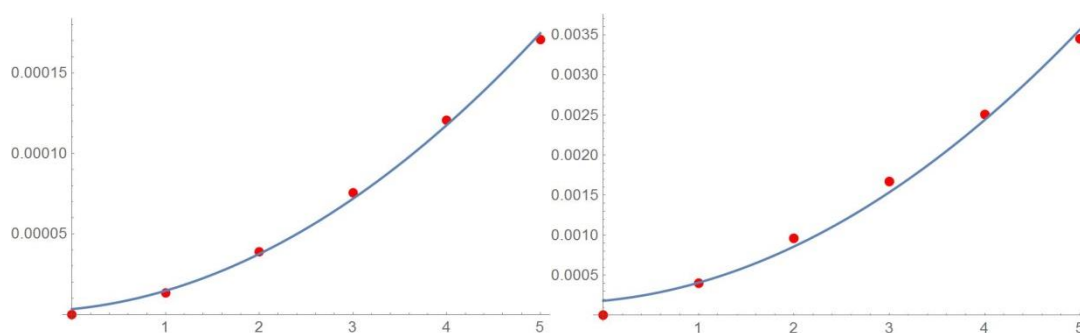


Fig. 35 CASSCF(left) and CASPT2(right) fits. ΔE (a.u.) vs. spin

The R values (correlation coefficients) are higher than 0,99 and so there is a good correlation between the data and the Heisenberg model. It is already remarkable that such a simple model gives such a good correlation. Nevertheless when we try to obtain the J value from only the energies from the two highest multiplicities we get the following blue lines:

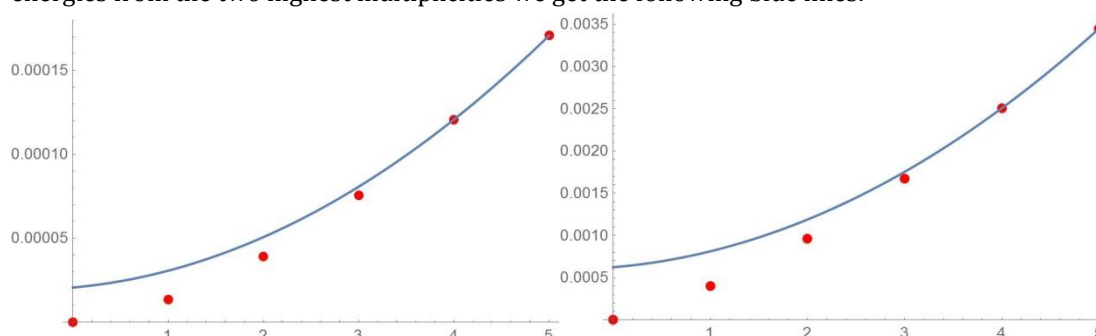


Fig. 36 CASSCF(left) and CASPT2(right) plots based on E_{9-11} (blue) and the calculated energies(red). ΔE (a.u.) vs. spin.

Here the value of the blue line at $S=0$ represents the expected energy that follows from the value obtained from the energy difference between multiplicity 9 and 11. This energy is too high. When the results of the three different ways are combined we get the following table:

Table 17 Energy differences from CASSCF calculations and CASPT2 calculations. Determined via the energy difference between singlet and undetctet(11), between nonet and undetctet, and from fit of all multiplicities

J couplings	E_{1-11} (a.u.)	E_{9-11} (a.u.)	E_{Fit} (a.u.)
CASSCF	-1,14E-05	-1,00E-05	-1,14E-05
CASPT2	-2,30E-04	-1,88E-04	-2,26E-04

The fit and the energy obtained by the difference of the lowest and highest multiplicity are approximately the same and the ΔE^{9-11} is approximately 15% higher. Nevertheless it gives a good idea about the magnetic coupling and we will now extrapolate this method to DDCI.

DDCI CALCULATIONS

DDCI calculations are performed also on cluster 3 with an ANO-L-VTZ basis set.

Table 18 DDCI results for MNMA, cluster 3 of the nonet and undetctet states

1,00E-11	DDCI1		DDCI2		DDCI3	
mult	E (a.u.)	ΔE (a.u.)	E (a.u.)	ΔE (a.u.)	E (a.u.)	ΔE (a.u.)
11	-7362,7699		-7362,7796		-7362,8208	
9	-7362,7718	-1,94E-03	-7362,7814	-1,82E-03	-7362,8227	-1,89E-03
J(a.u.)		-3,87E-04		-3,63E-04		-3,78E-04
J(meV)		-10,54		-9,88		-10,29

As expected the DDCI total energies are close to the CASSCF energy (high spin: -7362,7689 a.u.). Also we expected that the DDCI J couplings were larger than the ones obtained by CASSCF. They are even larger than the CASPT2 couplings. The DDCI1, DDCI2 and DDCI3 couplings are close together while it was expected that the couplings would increase going from DDCI1 to DDCI2 to DDCI3. For this reason the results are a bit strange. Especially for the DDCI1 case because we expected that the contribution of the singles would be small.

There are several ways to make the DDCI calculations more doable. The following options are considered:

1. Use a smaller basis set. (no f/g functions)
2. Freeze more orbitals (Mn 1s2s2p3s, Cl 1s2s2p3s)
3. Delete high virtual orbitals
4. Selected CI

In our calculations no f and g functions were used and for Mn the 3s orbitals were frozen. It was shown by earlier research that the effect of the f and g orbitals was very small.¹⁷ Instead of neglecting the f and g we could also use a stronger contraction. For example a VDZ basis could be used however in this case we lose a lot of flexibility of the basis set.

Another option is to freeze more orbitals. We froze the 3s orbitals of Cl and Mn. This is possible but did not give a significant lowering of the computer time. Also it is difficult to determine which orbitals to include and which not.

This problem is even larger when we consider deleting high level virtual orbitals. The virtual orbitals are usually quite close to each other and the energies are often not more than 1 a.u. higher than the HOMO energy level, hence it is difficult to place a cut-off from where to delete the higher orbitals. Also this is a very adhoc method without real scientific arguments; the only argument is the ease of computing. For this reason we did not delete higher orbitals because it is hard to justify where to place the boundary.

The DIESEL program package also gives us the possibility to do selected-CI. In this case a certain energy based cut-off value is given for the contribution of the CSFs. When the contribution is smaller than the cut-off value the coefficient of the determinant is set to zero. We tried a cut-off value on the single atom calculation but the results depended too much on the cut-off value varying it from 10^{-11} to 10^{-17} in steps of order of magnitude.

It would be very helpful to have more DDCI results in the future. Now the clusters are made it is mainly a matter of computer time to calculate J couplings via DDCI. Especially with obtaining the J values from only the highest two multiplicities it is now possible to obtain information on more complicated high spin clusters. Especially results for cluster 9 will be interesting to see if there is any intra layer coupling.

MNCL₄ PHENYL ETHYL AMINE

PERIODIC CALCULATION

To place the results of MNMA more in context also calculations are performed on MNPEA. This material has almost the same inorganic sheets although a much larger organic group. The same kind of periodic calculations were performed as with the MNMA crystal.

Table 19 Results of the periodic calculation on MNPEA

	total Energy	ΔE (a.u.)	ΔE (meV)	J(meV)	atomic spin density
FF	-14892,6420741	-	-	-	4,67 4,67 4,67 4,67
AA	-14892,6529277	-1,09E-02	-295,341	-2,95	-4,62 -4,62 4,62 4,62
FFA	-14892,6420741	-1,40E-08	-3,81E-04	-3,05E-05	-4,67 4,67 -4,67 4,67
FF GRIMME	-14892,6420745	-3,51E-07	-9,55E-03		

The J for the fully anti-ferromagnetic state is practically the same as for the MNMA state. From the spin densities it is seen that the spin densities on the manganese centers is a bit lower caused by the delocalization. These spin densities are not exactly -5 or 5 because there is always some spin delocalized towards the chlorine atoms.

The energy difference of the antiferromagnetic coupled sheets is even smaller than for MNMA, because the interlayer distance is very large.

Because the large phenyl groups in the crystal a Grimme correction is applied giving anyhow only a small energy lowering. This is smaller than expected because a calculation on benzene gave an energy lowering of more than 1 eV per benzene molecule.

DIFFERENT CLUSTERS

Also for the MNPEA a large sphere was made and the SCEI procedure was used to construct an AIMP for the manganese atoms. (appendix A) Because MNPEA has a buckling angle in both directions (110 and $\bar{1}10$) less clusters need to be built. Two clusters with two magnetic centers are built. Only cluster 2 includes the ligands. Clusters 4 and 5 were made including two manganese atoms from two different perovskite layers. Only cluster 5 is shown, cluster 4 is the same but does not include the PEA molecules.

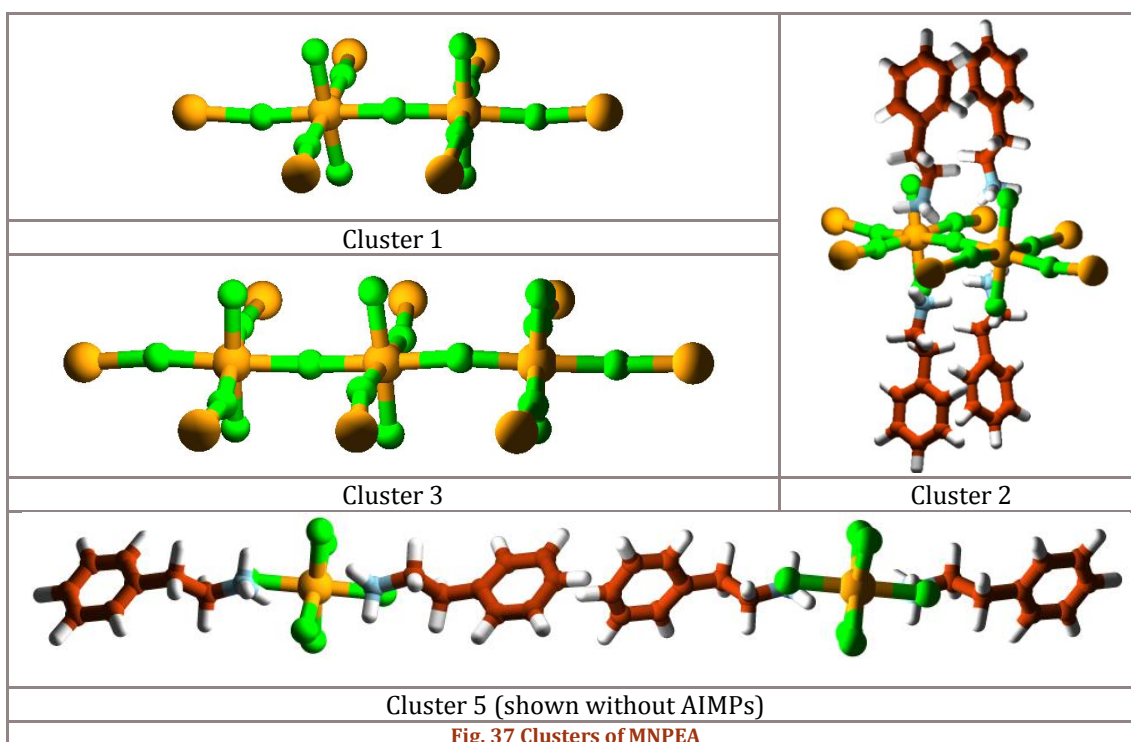


Table 20 Comparison of the periodic and embedded cluster calculation

	mult	Energy(a.u.)	ΔE (a.u.)	ΔE (meV)	npairs	n^*J	J (meV)
periodic:	11	-14892,6421					
	1	-14892,6529	-1,09E-02	-2,95E+02	8	25/2	-2,95
embedded:	11	-7369,69816					
	1	-7369,69959	-1,43E-03	-3,89E+01	1	25/2	-3,12

The J couplings were determined via DFT/PBE and the basis sets from the CRYSTAL basis set library. The calculations are reasonably close together although less similar than for the MNMA crystal. As expected the results do not differ significantly from the MNMA crystal.

RESULTS CASSCF&CASPT2

Table 21 CASSCF and CASPT2 energy differences of the MNPEA clusters. The energies are in meV.

J couplings (meV)	CASSCF		CASPT2	
	ANO-L-VTZ	ANO-RCC-VTZ	ANO-L-VTZ	ANO-RCC-VTZ
cluster 1	-0,299	-0,303	-7,03	-7,27
cluster 2	-0,302	-0,306	-	-
cluster 4	0	0	-0,68	-0,54
cluster 5	0	0	-	-

The CASSCF energies of the in-plane clusters are almost identical to the MNMA results. The CASPT2 energies are far too high, hence these results cannot be reliable.

It would be interesting to do DDCI calculations on the MNPEA crystal however we did not manage because of memory problems. We hope to find a very small J coupling between the layers because this is found experimentally below 50 K.⁵

FECL₄ METHYL AMINE

PERIODIC CALCULATION

Calculations are performed on a FEMA crystal to investigate the difference with the manganese based crystals. Again the same kind of periodic calculations are performed. The iron atoms have a d⁶ configuration and the high spin state becomes a nonet state, S=9.

Table 22 Results periodic calculation FEMA

	total E (a.u.)	ΔE (a.u.)	ΔE (eV)	$J_{16/2}$ (meV)	J (meV)
FM/FM	-13184,895087826	-	-	-	-
AFM/AFM	-13184,905443191	-0,0104	-0,2818	-35,2	-4,403
FM/FM/AFM	-13184,895086691	1,135E-06	3,088E-05	NA	0,0039

The in-plane J^{sing} coupling is -4,4 meV. This is larger than the J coupling of the manganese crystal that is approximately -3 meV. Because the Mn-Mn distance and Fe-Fe distances in the MNMA and FEMA crystal are practically the same this difference has to be explained otherwise. It is possible that the d orbitals of Fe²⁺ are larger than the d orbitals of Mn²⁺, in this case the overlap with the bridging chlorine atom is larger and hence there is a more efficient delocalization causing a larger stabilization of the low spin state.

The J coupling of anti-ferromagnetic coupled planes in FEMA is approximately 4 μ eV. Remarkably this is positive while this coupling in MNMA was negative. Although this is interesting, the coupling is so small that it is outside the accuracy range of our calculation and therefore it is not allowed to make any strong conclusions. In any case these interlayer interactions are very small and this gives us enough reasons to regard the perovskite planes as 2D magnets.

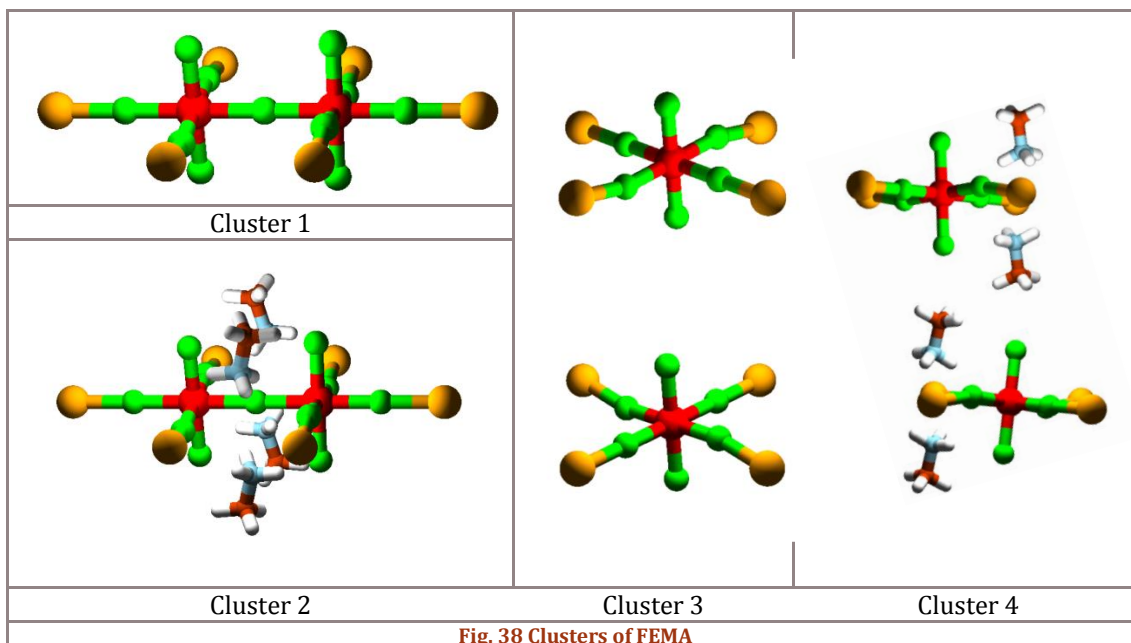
Table 23 Spin densities of the iron ions in FEMA

Spin Densities	1	2	3	4
FM/FM	3,6772	3,6772	3,6772	3,6772
AFM/AFM	-3,6313	3,6313	3,6313	-3,6313
FM/FM/AFM	3,6772	3,6772	-3,6772	-3,6772

The spin densities of the AFM/AFM state are lower. This is in agreement with the delocalization effect. Nevertheless this spin delocalization is not very large and almost all spin density stays located on the metal ions. The decrease in spin density is almost the same as for the MNPEA crystal.

DIFFERENT CLUSTERS

Again the AIMP procedure was followed to construct an iron-AIMP for the embedded cluster method in these crystals. In fig. 38 the clusters that are made for FEMA are shown. The red atoms show the iron atoms and the dark yellow atoms show the iron-AIMPs.



RESULTS CASSCF&CASPT2

CASSCF and CASPT2 calculations were performed on the FEMA crystal. To let the calculation converge first a $\text{Fe}^{3+} d^5$ calculation was performed to obtain correct start-up orbitals for the calculations.

Table 24 CASSCF and CASPT2 energy differences of the clusters of FEMA

J-couplings (meV)	CASSCF			CASPT2		
	L-VTZ	L-VTZp	RCC-VTZ	L-VTZ	L-VTZp	RCC-VTZ
ANO-						
cluster 1	-0,449	-0,420	-0,365	-1,34	-3,44	-2,77
cluster 2	-0,385	-0,387	-0,373	-	-	-
cluster 3	-2,54E-04	-	-7,44E-04	-1,53	9,95E-04	-1,77
cluster 4	-1,80E-03	-1,54E-03	-3,45E-04	-	-	-

The CASSCF results of cluster 1 and 2 are rather similar and the difference between them is small. For the ANO-L-VTZ and ANO-L-VTZp cluster 2 gives a smaller coupling however for ANO-RCC this is not the case. It seems that the inclusion of relativistic effects gives a slightly decrease of the coupling. The CASPT2 energy differences of cluster 1 are significantly higher than the CASSCF energies of clusters 1 and 2.

The CASSCF results of the clusters 3 and 4 are very small and there is not any significant difference between them. The CASPT2 results are again unrealistically high except for the ANO-L-VTZp result. Probably also here the CASPT2 suffered from intruder states and did converge to a wrong state.

OTHER CONSIDERATIONS

In all systems the interlayer magnetic couplings are very small. It is shown by M. Drillon and P. Panissod that the organic part can affect the interlayer coupling by dipole interactions causing a 3D magnetic ordering in the crystal. However they also showed that this 3D order was only present when the in-plane coupling was ferromagnetic. In the crystals studied the in-plane ordering was nevertheless anti-ferromagnetic and no 3D order is expected.³⁷

All the crystals show anti-ferromagnetic behavior as expected from the theory³² and confirmed by experiments.²⁵ When the bridging ligand is replaced by a point charge the J coupling decreases. This is also found in other calculations on other perovskite crystals.³⁵ There is no spin density on the amine cation group of the organic ligand. Hence the magnetic exchange is only due to the indirect exchange via the bridging halogen (Cl) ligands.

There is only a slight difference between the MNMA and MNPEA crystals. The in-plane coupling is almost identical while the intra-layer couplings are very small in both cases. The difference in electric properties will probably be much more pronounced. DDCI calculations of inter layer clusters with the organic part included ought to be performed to decide whether there is a significant different magnetic behavior between these crystals.

For the in-plane clusters the J couplings of FEMA ($\sim -0,4$ meV) are larger than the J couplings of the MNMA crystal ($\sim -0,3$ meV). Because the distance between the metal centers are the same it can possibly be caused by the larger overlap of iron with the bridging ligands. When the d orbitals of iron are larger there is a larger interaction with the orbitals on the chlorine atoms and so a more efficient indirect exchange. The indirect exchange goes mainly via the p_x orbital on the bridging chlorine atom that is parallel to the Mn-Cl-Mn bond. The energy of this orbital that is mainly the p_x orbital on the bridging Cl atom can also influence the exchange. The closer the energy of this orbital to the d orbitals on the metal atom, the more efficient is the exchange process. The p_x orbital energy for MNMA/SCF/S=11 is $-0,68$ a.u. while the p_x orbital energy for FEMA/SCF/S=9 is $-0,53$ a.u. (the energies of the d orbitals are considered to be at $E=0$.)

In our group calculations were performed on $\text{CuCl}_4(\text{C}_2\text{H}_5\text{NH}_3)_2$ (CUEA), that gave a ferromagnetic result with the same embedded cluster methodology and CASSCF/DDCI calculations. The J couplings for CUEA were around $0,18$ meV for CASSCF. Our CASSCF calculations on MNMA gave J couplings around $-0,30$ meV, and $-0,40$ meV for FEMA. So the absolute J coupling of manganese and iron is larger. The DDCI calculations on CUEA were around $0,2-0,7$ meV. This is larger than the CASSCF results of CUEA but still very close while our DDCI values were an order of magnitude larger than the CASSCF results.³⁸

In the near future it is advised to do a further investigation of the interlayer couplings on all the crystals with DDCI on the highest multiplicities. This will provide us more certainty about the interlayer effects.

Further research on OIHs is advised to cover perovskites with ferromagnetic couplings within the layer, or to use organic molecules with small organic or π -conjugated molecules. Also a lot of lead-iodine based OIHs are investigated nowadays.

CONCLUSION

A detailed analysis of the magnetic coupling in two-dimensional hybrids is given. The manganese and iron based hybrids have an anti-ferromagnetic in-plane coupling. The interlayer couplings are obviously an order of magnitude smaller than the intralayer couplings. The embedded cluster model was well validated by reproducing the same magnetic couplings as the periodic calculations.

As expected the CASPT2 results artificially overestimate the magnetic couplings while the CASSCF results underestimated the couplings. The DDCI method shows a large magnetic coupling but for the DDCI still further investigations are needed. At least the embedded clusters are already constructed and a method to obtain a J coupling from the highest multiplicities has been formulated and validated.

MNMA and MNPEA have almost the same magnetic character; this emphasizes the 2D character of these crystals, because a change in organic ligand from aliphatic to aromatic and from a small to a large organic group has only small effects. MNMA and FEMA show the same anti-ferromagnetic ordering. But the J coupling of the iron crystals is higher.

ACKNOWLEDGEMENTS

First of all I would like to thank Remco Havenith. His guidance was very helpful and he was always open for questions. Several times he challenged me to look from different perspectives. Secondly I want to thank Ria for her supervision and discussion on magnetic interactions. Also I am grateful that I could attend a Jujols workshop in Germany and the Physics@FOM conference in Veldhoven.

During this master project I joined the office first together with Andrii and later on together with Hilde. I thank both for the useful and also pleasant conversations. I also thank Gerrit-Jan Linker for the fruitful discussions on various topics, especially on the CRYSTAL program. Also I have to thank Jeroen teaching me to use awk and sed scripts. This was very helpful and saved me a lot of tedious work.

Last but certainly not least I thank SurfSara for using their computer systems to perform large calculations. It was a good experience to use this large supercomputing facility.

REFERENCES

1. P. S. Ghalsasi, K. Inoue, *Polyhedron*, **2009**, 28, 1864-1867
2. P. Rabu, M. Drillon, *Adv. Eng. Mat.* **2003**, 5, 4, 189-210
3. C.N.R. Rao, A.K. Cheetham, A. Thirumurugan *J. Phys.: Condens. Matter* **2008**, 20, 83202
4. D.B. Mitzi, *Prog. Inorg. Chem.*, **1991**, 48, 1
5. A. Arkenbout *Organic-Inorganic Hybrids, a route towards Soluble Magnetic Electronics*, Rijksuniversiteit Groningen, Rijksuniversiteit Groningen, **2010**
6. L. Guo, S. Xu, G. Zhao, H. Liu, *J. Phys. Chem. Sol.*, **2012**, 73, 688-695
7. L. Guo, Z. Sun, G. Zhao, X. Li, H. Liu, J. Wuhan, *U. Tech-Mater. Sci. Ed.*, **2012**, 27, 5, 957-961
8. A Hypertext Book of Crystallographic Space Group Diagrams and Tables, Department of Chemistry, Birkbeck College, London, **1997**, retrieved from <http://img.chem.ucl.ac.uk>
9. H. Arend, K. Tichy, K. Baberschke, F. Rys, *Solid State Comm.*, **1976**, 18, 999-1003
10. C.B. Aakeröy, T.A. Evan, K.R. Seddon, I. Pálinkó, *New J. Chem.*, **1999**, 145-152
11. R. Dovesi, R. Orlando, B. Civalleri, C. Roetti, V. R. Saunders, and C. M. Zicovich-Wilson, *Z. Kristallogr.* **2005**, 220, 571
12. R. Dovesi, V. R. Saunders, C. Roetti, R. Orlando, C. M. Zicovich-Wilson, F. Pascale, B. Civalleri, K. Doll, N. M. Harrison, I. J. Bush, P. D'Arco, and M. Llunell, *CRYSTAL09 User's Manual* (University of Torino, Torino, **2009**).
13. A.L.Spek, *Acta Cryst.* **2009**, 65, 148-155.
14. J.P. Perdew, K. Burke, M. Ernzerhof, *Phys. Rev. Lett.* **1996**, 77, 3865-3868
15. P.O. Widmark, **2011**, *European Summerschool in Quantum Chemistry 2011*, 7th ed., University of Lund, Lund, Sweden
16. S. Grimme, *J. Comput. Chem.*, **2004**, 25, 1463-1473
17. A. M. Pradipto, *Local Interactions in Magnetic and Ferroelectric Materials: Magnetic and Vibronic Couplings*, Rijksuniversiteit Groningen, **2013**
18. B. Roos, U. Wahlgren. Institute of Theoretical Physics, University of Stockholm, **1969**, turbo version, **1970**
19. J.L. Pascual, N. Barros, Z. Barandiarán, L. Seijo *J. Phys. Chem. A* **2009**, 113, 12454-12460
20. B. Swerts, L. Chibotaru, R. Lindh, L. Seijo, Z. Barandiarán, S. Clima, K. Pierloot, M.F.A. Hendrickx, *J. Chem. Theory Comput.* **2008**, 4, 586-594
21. F. Aquilante, L. De Vico, N. Ferré, G. Ghigo, P.-Å Malmqvist, P. Neogrady, T.B. Pedersen, M. Pitonak, M. Reiher, B.O. Roos, L. Serrano-Andrés, M. Urban, V. Veryazov, R. Lindh, *J. Comput Chem.*, **2010**, 31, 224
22. M. Hanrath, B. Engels. *Chem. Phys.* **1997**, 225, 197
23. N. Forsberg P. Malmqvist, *Chem. Phys. Lett.* **1997**, 274, 196-204
24. J. Cabrero, E. Bordas, C. De Graaf, M. Reguero, R. Caballol, *The Difference-Dedicated Configuration Interaction method: an accurate procedure to calculate energy transitions*, Universitat Rovira I Virgili, **2001**

25. I.P.R. Moreira, F. Illas, J. Calzado, J.F. Sanz, J.-P. Malrieu, N. Ben Amor, D. Maynau, Phys. Rev. B, **1999**, 59, 10, 6593-6596
26. F. Illas, I.P.R. de Moreira, C. de Graaf, B. Vincenzo, Theor. Chem. Acc. **2000**, 104, 265-272
27. C. de Graaf, C. Sousa, I. de P.R. Moreira, F. Illas, J. Phys. Chem. A **2001**, 105, 11371-11378
28. B.O. Roos, R. Lindh, P.-Å. Malmqvist, V. Veryazov, P.-O. Widmark, J. Phys. Chem. A, **2005**, 109, 6575-6579
29. S. J. Leon, **2000**, *Linear Algebra 8th ed., Ch. 6* Upper Sadle River, NJ, USA, Pearson
30. D. Dai, M.H. Whanbo, J. Chem. Phys., **2003**, 118, 1, 29-39
31. I.P.R. Moreira, F. Illas, Phys. Chem. Chem. Phys., **2006**, 8, 1645-1659
32. J. Kanamori, J. Phys. Chem. Solids **1959**, 10, 87-98
33. P. Zolfaghari, G.A. de Wijs, R.A. de Groot, J. Phys.: Condens. Matter **2013**, 25, 295502
34. J.P. Malrieu, R. Caballol, C.J. Calzado, C. de Graaf, N. Guihéry, Université de Toulouse, *Magnetic interactions in molecules and highly correlated materials: Physical content, analytical derivation and rigorous extraction of magnetic Hamiltonians.*
35. C. de Graaf, *Local Excitations and Magnetism in late Transition Metal Oxides, Rijksuniversiteit Groningen, 1998*
36. N. Queralt, D. Taratiel, C. de Graaf, R. Caballol, R. Cimiraglia, C. Angeli J. Comput. Chem. **2008**, 29, 994-1003
37. M. Drillon, P. Panisod J. Magn. Magn. Mat. **1998**, 188, 93-99
38. L. Cusinato, Magnetic interactions in organic-inorganic hybrid copper materials, **2013**, Rijksuniversiteit Groningen.

APPENDICES

- A. Coordinates of the crystals
- B. AIMP's of MNMA/MNPEA/FEMA
- C. Manual to make AIMP's etc.
- D. Data-sets

APPENDIX A – CRYSTAL STRUCTURES

MNMA

_cell_length_a	7.1999(2)
_cell_length_b	7.1999(2)
_cell_length_c	19.2744(7)
_cell_angle_alpha	90.00
_cell_angle_beta	90.00
_cell_angle_gamma	90.00
_cell_volume	999.16(5)

1	T	MN	0.000000	0.000000	-0.500000
5	T	CL	0.031610	0.031610	-0.371740
13	T	CL	0.250000	0.250000	0.481340
17	T	CL	-0.250000	0.250000	-0.500000
21	T	C	-0.030300	-0.030300	0.187650
29	T	N	0.017600	0.017600	0.115670
37	T	H	-0.001780	-0.175763	0.195471
53	T	H	0.053162	0.053162	0.221918
61	T	H	0.154058	-0.005443	0.106948
77	T	H	-0.057169	-0.057169	0.081299

MNPEA

_cell_length_a	7.1480(6)
_cell_length_b	7.1697(7)
_cell_length_c	39.088(4)
_cell_angle_alpha	90.00
_cell_angle_beta	90.00
_cell_angle_gamma	90.00
_cell_volume	2003.2(3)

1	T	MN	0.009120	0.499710	0.000020
5	T	CL	-0.024600	0.499200	0.063280
9	T	CL	0.236700	0.221000	0.004800
13	T	CL	0.284700	-0.262700	0.007030
17	T	CL	0.042300	0.480900	-0.063290
21	T	N	-0.486500	0.491400	0.059840
25	T	N	-0.002200	-0.029400	0.059300
29	T	C	0.119500	-0.098000	0.179700
33	T	C	0.466900	-0.455200	0.093500
37	T	C	-0.457000	0.404000	0.120900
41	T	C	-0.482000	0.478000	0.157900
45	T	C	-0.365000	-0.386000	0.169600
49	T	C	-0.378000	-0.332000	0.202500
53	T	C	0.481000	-0.384000	0.222000
57	T	C	0.361800	0.464000	0.211300
61	T	C	0.380000	0.395000	0.176600
65	T	C	0.051300	0.032600	0.095900
69	T	C	-0.042000	-0.093600	0.120900
73	T	C	-0.013600	-0.029000	0.156600
77	T	C	-0.136000	0.106000	0.171500
81	T	C	-0.122000	0.170000	0.204100
85	T	C	0.027300	0.092000	0.224500
89	T	C	0.139000	-0.027000	0.215200
93	T	H	0.475637	0.354045	0.054402
97	T	H	-0.341224	0.498178	0.055982
101	T	H	0.447735	-0.422485	0.041680
105	T	H	0.313354	-0.444710	0.095645
109	T	H	-0.475808	-0.315066	0.098346

113	T	H	0.471529	0.268743	0.118102
117	T	H	-0.307108	0.380197	0.115337
121	T	H	-0.250509	-0.336280	0.153411
125	T	H	-0.281426	-0.221539	0.211166
129	T	H	0.465142	-0.330808	0.248222
133	T	H	0.249219	0.414362	0.228039
137	T	H	0.291319	0.280134	0.167510
141	T	H	-0.144278	-0.003366	0.055183
145	T	H	0.017931	-0.172021	0.056069
149	T	H	0.077714	0.043163	0.041019
153	T	H	0.205183	0.025466	0.097341
157	T	H	0.007709	0.179197	0.098292
161	T	H	-0.193685	-0.097908	0.115206
165	T	H	0.011315	-0.237297	0.117586
169	T	H	-0.251057	0.159585	0.155599
173	T	H	-0.214538	0.279841	0.213703
177	T	H	0.036051	0.151725	0.250569
181	T	H	0.254605	-0.082921	0.230470
185	T	H	0.218614	-0.208237	0.171948

FEMA

_cell_length_a	7.1325(6)
_cell_length_b	7.1325(6)
_cell_length_c	19.0193(17)
_cell_angle_alpha	90.00
_cell_angle_beta	90.00
_cell_angle_gamma	90.00
_cell_volume	967.56(14)
_cell_formula_units_Z	4
_cell_measurement_temperature	100(2)

1	T	FE	0.000000	0.000000	0.000000
5	T	CL	0.250000	-0.250000	0.000000
9	T	CL	0.026200	0.026200	-0.125830
17	T	CL	0.250000	0.250000	0.016000
21	T	N	-0.488500	-0.011500	0.113700
29	T	C	0.475200	0.024800	0.188000
37	T	H	0.073257	-0.105495	-0.287276
53	T	H	0.133074	0.133074	-0.306734
61	T	H	0.107460	-0.059447	-0.412318
77	T	H	-0.113623	-0.113623	-0.391378

APPENDIX B – AIMPS

AIMP – MNMA – MN

/Mn.ECP.Jos.0s.0s.0e-Mn(MnCl4MA).

first comment

second comment

2.000 0

0 0

*

* External AIMP:

* Local Pot. Param. : (ECP convention)

A(AIMP)=-Zeff*A(ECP)

*

M1

12

328944.7000	45167.27200	9923.015200	2666.068200
827.1021100	279.6520400	89.07853200	34.35214600
13.85860570	3.948510300	1.748313600	0.9893750000E-01
0.9215318818E-01	0.1210537800	0.2242009432	0.3999195333
0.6505229958	0.7977148609	1.147662441	2.133239869
1.017765206	2.825318731	2.036960289	0.5348816188E-01

M2

0

COREREP

1.000

PROJOP

2

20	3	2	2	2
480.4698533	58.24983595	7.430899373		
3960805.000	593115.5000	134976.8000	38230.67000	

```

12471.54000      4501.743000      1755.212000      727.3039000
316.3678000     143.0098000     66.21805000     29.91896000
14.30318000     6.839451000     3.012374000     1.418808000
0.6236240000    0.1340980000    0.6554800000E-01 0.2958400000E-01
0.000134806316 -0.000041936084 -0.000015746414
0.000533182211 -0.000166541817 -0.000062407290
-0.000166686538 0.000056341748 0.000021178002
0.001912532908 -0.000583335091 -0.000218806136
0.005177837185 -0.001570671820 -0.000587601677
0.017737526639 -0.005442432723 -0.002046509373
0.049781670225 -0.015638478322 -0.005868621287
0.124024350821 -0.041069646300 -0.015600246550
0.250365724259 -0.092986163635 -0.035536999727
0.358892022166 -0.168614609750 -0.067082645103
0.275683421884 -0.189280182524 -0.077939360078
0.066049166661 0.045928875025 0.018193620488
-0.000930447851 0.515004405759 0.310996237696
0.002300920231 0.504695773814 0.462362741405
-0.000905936966 0.090626206715 -0.119000504485
0.000271760038 -0.001783084852 -0.791275278538
-0.000238101870 0.001908386124 -0.339083371678
0.000069677537 -0.000627026220 -0.002083501063
-0.000004557538 0.001623579677 -0.051671148770
0.000010425754 -0.000879829042 0.030454170290
 16   2   6   6
49.70985852      4.685918126
16205.86000      3836.274000      1246.048000      476.7535000
202.1895000      92.09487000      44.14720000      21.85468000
11.08596000      5.674108000      2.823170000      1.368621000
0.6444310000     0.2483460000     0.9717500000E-01 0.3656500000E-01
0.000041770506 -0.000015396437
0.000371807153 -0.000136795571
0.002143273618 -0.000792781203
0.009418233515 -0.003495487694
0.033197615470 -0.012517758023
0.094466490623 -0.036464303110
0.207448472108 -0.083464401369
0.330888034830 -0.139335791091
0.332469462326 -0.146399141780
0.157569769798 0.030828248757
0.023558846618 0.346215466383
0.001036594544 0.487782253302
0.000271362366 0.245796443372
-0.000015237875 0.018992446031
0.000145290456 0.026487705748
-0.000066733881 -0.013167262464
  8   1   5
-.9814859686E-01
101.9040000      30.03370000      10.92380000      4.397400000
1.815950000      0.7257310000     0.2699610000     0.8776000000E-01
-0.004388012898
-0.031782041491
-0.123609250954
-0.295134107878
-0.451659504475
-0.418100745228
0.242657975365
-0.214080723994

```

```

*
Spectral Representation Operator
Core primitive basis
Exchange
End of Spectral Representation Operator

```

AIMP - MNMA - CL

```
/Cl.ECP.Jos.0s.0s.0e-Cl(MnCl4MA).
```

```
first comment
```

```
second comment
```

```
-1.000  0
  0  0
```

```
*
```

```
* External AIMP:
```

```
* Local Pot. Param. : (ECP convention)
```

```

*
*
*
M1
12
279010.5000      33072.04800      6508.195100      1639.626100
486.4457200      161.2054900      50.60618900      17.72200500
7.448597800      0.6676690000     1.664862400      0.2679957200
-.1218520375     -.1800615700     -.3434006915     -.6235520182
-1.057669238     -1.363008766     -1.585242202     -3.276129124
-2.748551671     -3.396635409     -1.996537633     -1.307359641
M2
0
COREREP
1.000
PROJOP
2
15 3 2 2 2
208.2081990      19.66090406      0.7114134176
456100.0000      68330.00000      15550.00000      4405.000000
1439.000000      520.4000000      203.1000000      83.96000000
36.20000000      15.83000000      6.334000000      2.694000000
0.9768000000     0.4313000000     0.1625000000
0.000049296561   0.000013826074   0.000004052446
0.000383025037   0.000107246440   0.000031378213
0.002008518868   0.000564904658   0.000165739607
0.008385501076   0.002360639152   0.000690483303
0.029470013083   0.008456146839   0.002487812229
0.087831788707   0.025956035406   0.007618645871
0.211470958016   0.068612867440   0.020452009612
0.365354350924   0.141825745733   0.042649977555
0.340879441988   0.199223272468   0.063411666288
0.102150943154   0.019642847091   0.004960845260
0.003124069829   -0.499359999584   -0.196934470524
0.001056413337   -0.563786743365   -0.395519217924
-0.000378479455   -0.079284276932   0.085947163152
0.000153761101   0.008317102572   0.631968675467
-0.000051990977   -0.002650526475   0.475967185758
9 2 6 6
14.59304649      -.4574903643
663.3000000      156.8000000      49.98000000      18.42000000
7.240000000      2.922000000      1.022000000      0.3818000000
0.1301000000
-0.002405390710   0.000596565221
-0.019221824136   0.004747204158
-0.088544918974   0.022589439468
-0.256094594484   0.066507920408
-0.437127440903   0.122719068171
-0.350535706841   0.087099066932
-0.058082390743   -0.236389530677
0.005360532753   -0.505530375789
-0.001750101346   -0.430274700734
2 1 0
-2.418353729
1.046000000      0.3440000000
-0.132137282686
-0.915439962151

```

```

*
Spectral Representation Operator
Core primitive basis
Exchange
End of Spectral Representation Operator

```

AIMP - MNPEA - MN

/Mn.ECP.Jos.0s.0s.0e-Mn(MnCl4PEA).

first comment

second comment

2.000 0

0 0

*

* External AIMP:

* Local Pot. Param. : (ECP convention)

* A(AIMP)=-Zeff*A(ECP)

*

M1

12

330339.4200	45514.68700	10013.19780	2689.893200
834.4033900	281.9965800	89.43293500	34.41922800
14.03163420	3.903915800	1.643823270	0.5846364200
0.9085398774E-01	0.1190518295	0.2206866581	0.3938565529
0.6415461579	0.7874833736	1.128202521	2.102322023
0.9782919044	2.629659303	1.989662519	0.4183831691

M2

0

COREREP

1.000

PROJOP

2

20	3	2	2	2			
481.0364353			58.75400289		8.030896428		
3960805.000			593115.5000		134976.8000		38230.67000
12471.54000			4501.743000		1755.212000		727.3039000
316.3678000			143.0098000		66.21805000		29.91896000
14.30318000			6.839451000		3.012374000		1.418808000
0.6236240000			0.1340980000		0.6554800000E-01		0.2958400000E-01
0.000134807438			-0.000041929786		-0.000015807543		
0.000533186024			-0.000166516292		-0.000062699919		
-0.000166681730			0.000056322048		0.000021927879		
0.001912569352			-0.000583274569		-0.000217580134		
0.005177948757			-0.001570588705		-0.000582043980		
0.017737948314			-0.005441928278		-0.002028440373		
0.049782770069			-0.015637766151		-0.005818306154		
0.124028043836			-0.041066029511		-0.015457468717		
0.250372685760			-0.092985460292		-0.035238615525		
0.358909392493			-0.168603399515		-0.066441315691		
0.275680856206			-0.189299341495		-0.077341738711		
0.066014532675			0.046160518893		0.018419494470		
-0.000935939280			0.514679957126		0.307062139540		
0.002306485935			0.504628750857		0.457207948626		
-0.000906812840			0.090701286593		-0.116232789397		
0.000278667123			-0.001399111709		-0.760270240000		
-0.000243644011			0.001780235878		-0.375854624414		
0.000083237941			0.000132263631		-0.033438439417		
-0.000041159925			-0.000556020806		0.034718264597		
0.000025221667			0.000007166436		-0.004453810635		
16	2	6	6				
50.22587896			5.382255015				
16205.86000			3836.274000		1246.048000		476.7535000
202.1895000			92.09487000		44.14720000		21.85468000
11.08596000			5.674108000		2.823170000		1.368621000
0.6444310000			0.2483460000		0.9717500000E-01		0.3656500000E-01
0.000041773374			0.000015154329				
0.000371827462			0.000134606360				
0.002143435670			0.000780303153				
0.009418942886			0.003439500506				
0.033201428947			0.012320210155				
0.094479176179			0.035875134451				
0.207490126545			0.082137405471				
0.330821126461			0.136941332152				
0.332246971428			0.143807734873				
0.157655482009			-0.029606795180				
0.023774058898			-0.335235468938				
0.001238775892			-0.474470553241				
0.000293435102			-0.267880468437				
-0.000103829772			-0.040885039199				
0.000042358079			0.009438385374				
-0.000027745792			0.005276536674				
8	1	5					
0.6462398554							
101.9040000			30.03370000		10.92380000		4.397400000
1.815950000			0.7257310000		0.2699610000		0.8776000000E-01
0.003541301287							
0.025812911893							
0.099519654741							
0.239558479195							
0.363128140893							
0.371051942257							

0.269004427420
 -0.077948915453
 *
 Spectral Representation Operator
 Core primitive basis
 Exchange
 End of Spectral Representation Operator

AIMP - FEMA - FE

/Fe.ECP.Jos.0s.0s.0e-Fe(FeCl4MA).

first comment
 second comment

2.000 0
 0 0

*
 * External AIMP:
 * Local Pot. Param. : (ECP convention)
 * A(AIMP)=-Zeff*A(ECP)
 *

M1

12				
317027.2100	42242.78800	9075.611000	2394.738900	
737.3620700	243.1891400	76.20894500	30.58243400	
9.593285900	3.577150600	1.434564140	0.4657483100	
0.9863979599E-01	0.1327199404	0.2493392217	0.4480407968	
0.7082571112	0.8327225367	1.413438051	2.119459938	
0.9810127902	3.037940264	1.633136344	0.3452932098	

M2

0
 COREREP
 1.000

PROJOP

2				
20	3	2	2	2
522.4031982	64.19575656	8.598326587		
4316265.000	646342.4000	147089.7000	41661.52000	
13590.77000	4905.750000	1912.746000	792.6043000	
344.8065000	155.8999000	72.23091000	32.72506000	
15.66762000	7.503483000	3.312223000	1.558471000	
0.6839140000	0.1467570000	0.7058300000E-01	0.3144900000E-01	
-0.000141110870	0.000044245131	0.000016853765		
-0.000556983309	0.000175379645	0.000066761204		
0.000197263338	-0.000066701095	-0.000026447617		
-0.001920724579	0.000589657768	0.000221069337		
-0.005116320870	0.001560273784	0.000580601394		
-0.017603497759	0.005431537904	0.002029740164		
-0.049379138603	0.015597214361	0.005832869614		
-0.123188158398	0.041010949658	0.015466011350		
-0.249158358546	0.093014054842	0.035468607191		
-0.358515050099	0.169144028491	0.066696666595		
-0.277240666331	0.191042938287	0.078983808716		
-0.067244178452	-0.043884173333	-0.018939935949		
0.000811266187	-0.515537305519	-0.307125960748		
-0.002310195231	-0.504952656175	-0.463028934950		
0.000876650358	-0.092233024765	0.131077295818		
-0.000236444945	0.002166649536	0.736693598592		
0.000231357766	-0.002536832126	0.391780811329		
-0.000077822993	-0.000128800069	0.040038451441		
0.000049675801	0.001054308850	-0.058549905894		
-0.000036645292	-0.000374055375	0.020224880593		
16	2	6	6	
55.23203367	5.762934174			
17745.69000	4200.721000	1364.429000	522.0806000	
221.4595000	100.9096000	48.40115000	23.98536000	
12.18250000	6.242298000	3.110944000	1.509958000	
0.7108450000	0.2725980000	0.1039720000	0.3816600000E-01	
-0.000041360978	0.000015105761			
-0.000368212592	0.000134275896			
-0.002123846358	0.000778419643			
-0.009344687754	0.003437746541			
-0.033008858073	0.012334449675			
-0.094173003872	0.036041301867			
-0.207477700663	0.082779743356			

ANO-RCC-VTZ(p)	CASSCF			CASPT2	
	mult	E(a.u.)	ΔE (a.u.)	E(a.u.)	ΔE (a.u.)
Cluster 3	11	-7393,290739		-7396,407841	
	1	-7393,290886	-1,47E-04	-7396,412010	-4,17E-03
Cluster 4	11	-7393,294225		-7395,651251	
	1	-7393,294395	-1,71E-04	-7395,654696	-3,44E-03
Cluster 6	11	-7778,373770		-7782,343490	
	1	-7778,373920	-1,50E-04	-7782,346933	-3,44E-03
Cluster 7	11	-7778,371569		-7782,343836	
	1	-7778,371741	-1,72E-04	-7782,347291	-3,46E-03
Cluster 8	11	-7856,982462		-7860,291475	
	1	-7856,982462	0	-7860,292593	-1,12E-03
Cluster 9	11	-8242,867329		-8246,973875	
	1	-8242,867329	-3E-08	-8246,974315	-4,41E-04

MNPEA

ANO-L-VTZ(p)	mult	CASSCF		CASPT2	
		E(a.u.)	ΔE (a.u.)	E(a.u.)	ΔE (a.u.)
cluster 4	11	-7362,737930		-7365,783680	
	1	-7362,738095	-1,65E-04	-7365,787553	-3,87E-03
cluster 6	11	-8822,149216		-	
	1	-8822,149383	-1,67E-04	-	
cluster 8	11	-7824,536390		-7827,015037	
	1	-7824,536390	-1,E-08	-7827,015415	-3,78E-04
cluster 9	11	-9284,604524		-	
	1	-9284,604525	-1,E-07	-	

ANO-RCC-VTZ(p)	CASSCF			CASPT2	
	mult	E(a.u.)	ΔE (a.u.)	E(a.u.)	ΔE (a.u.)
cluster 4	11	-7393,249801		-7396,368850	
	1	-7393,249968	-1,67E-04	-7396,372855	-4,01E-03
cluster 6	11	-8852,895166		-	
	1	-8852,895335	-1,69E-04	-	
cluster 8	11	-7856,474995		-7859,018832	
	1	-7856,474995	-7,E-08	-7859,019127	-2,96E-04
cluster 9	11	-9316,738466		-	
	1	-9316,738467	-1,E-07	-	

FEMA

ANO-L-VTZ(p)	CASSCF			CASPT2	
	mult	E(a.u.)	ΔE (a.u.)	E(a.u.)	ΔE (a.u.)
X4	9	-7588,027548		-7590,437482	
	1	-7588,027796	-2,48E-04	-7590,438219	-7,37E-04
X6	9	-7972,984593		-	
	1	-7972,984806	-2,12E-04	-	
X8	9	-8050,360679		-8052,929619	
	1	-8050,360679	-1E-07	-8052,930465	-8,45E-04
X9	9	-8436,120242		-	
	1	-8436,120243	-1E-06	-	

ANO-L-pVTZ-fg	CASSCF		CASPT2		
	mult	E(a.u.)	ΔE (a.u.)	E(a.u.)	ΔE (a.u.)
X4	9	-7588,043393		-7591,238977	
	1	-7588,043625	-2,32E-04	-7591,240872	-1,89E-03
X6	9	-7972,999647		-	
	1	-7972,999861	-2,14E-04	-	
X8	9	-8050,376903		-8052,929620	
	1	-8050,383955	-7,05E-03	-8052,929620	5E-07
X9	9	-8436,136709		-	
	1	-8436,136709	-8E-07	-	

ANO-RCC-VTZ(p)	CASSCF		CASPT2		
	mult	E(a.u.)	ΔE (a.u.)	E(a.u.)	ΔE (a.u.)
X4	9	-7621,299047		-7623,742493	
	1	-7621,299248	-2,01E-04	-7623,744023	-1,53E-03
X6	9	-8006,371279		-	
	1	-8006,371485	-2,06E-04	-	
X8	9	-8085,046022		-8087,640632	
	1	-8085,046022	-4E-07	-8087,641607	-9,75E-04
X9	9	-8470,922384		-	
	1	-8470,922384	-2E-07	-	

mult	CASSCF (a.u.)	CASPT2 (a.u.)	ΔE CASSCF (a.u.)	ΔE CASPT2 (a.u.)
9	-7621,299047	-7623,742489	2,04E-04	1,34E-03
7	-7621,299122	-7623,742748	1,28E-04	1,08E-03
5	-7621,299182	-7623,743167	6,82E-05	6,65E-04
3	-7621,299228	-7623,743593	2,24E-05	2,39E-04
1	-7621,29925	-7623,743833	0,00E+00	0,00E+00

DDCI Mn²⁺

mult	DDCI _n	Energy (a.u.)	nCSF	nConf
6	DDCI1	-1149,107239	522	192
	DDCI2	-1149,167904	726	396
	DDCI3	-1149,229218	3756	951
4	DDCI1	-1148,962644	7478	2282
	DDCI2	-1149,025685	9949	3247
	DDCI3	-1149,087463	28270	5955
2	DDCI1	-1148,899155	13934	4542
	DDCI2	-1148,956757	18564	6163
	DDCI3	-1149,019094	55620	12760

DDCI MnCl₆⁴⁻

mult	DDCI _n	Energy(a.u.)	nCSF	nConf
6	DDCI1	-3906,834128	21846	4296
	DDCI2	-3906,896255	39523	21973
	DDCI3	-3907,000268	1833839	327369
4	DDCI1	-3906,717016	337814	79226
	DDCI2	-3906,790159	426307	116158
	DDCI3	-3906,900184	5269354	913224
2	DDCI1	-3906,664773	625730	186126
	DDCI2	-3906,741364	792848	242241
	DDCI3	-3906,855152	10643670	2061982

DDCI Fe²⁺

mult	DDCI	Energy(a.u.)	nCSF	nConf
5	DDCI1	-1261,708111	4535	1655
	DDCI2	-1261,936731	255200	65678
	DDCI3	-1261,886894	519690	89147
3	DDCI1	-1261,646875	22875	7145
	DDCI2	-1261,831858	842163	158363
	DDCI3	-1261,778449	1858001	295102
1	DDCI1	-1261,602408	16370	8505
	DDCI2	-1261,784099	523271	176058
	DDCI3	-1261,730717	1140728	342927